Master Thesis
TVVR 19/5005

Flow simulation in MIKE URBAN based on high-resolution X-band radar data

A case study in Lund

Lisa Olsson


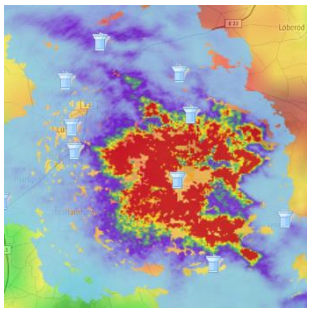


Division of Water Resources Engineering
Department of Building and Environmental Technology
Lund University

Flow simulation in MIKE URBAN based on high-resolution X-band radar data

A case study in Lund

By:
Lisa Olsson
Environmental Engineering (Ekosystemteknik)

Master Thesis

Division of Water Resources Engineering
Department of Building & Environmental Technology
Lund University
Box 118
221 00 Lund, Sweden

Water Resources Engineering
TVVR-19/5005
ISSN 1101-9824

Lund 2019
www.tvrl.lth.se

Master Thesis
Division of Water Resources Engineering
Department of Building & Environmental Technology
Lund University

English title:	*Flow simulation in MIKE URBAN based on high-resolution X-band radar data*
Swedish title:	*Flödesmodellering i MIKE URBAN baserad på högupplöst X-bandradardata*
Author:	Lisa Olsson
Supervisor:	Magnus Persson, LTH; Steve Berggren-Clausen, DHI
Examiner:	Rolf Larsson, Water Resources Engineering LTH
Language	English
Year:	2019
Keywords:	X-band radar; MIKE URBAN; modelling; rainfall-runoff; online control

Acknowledgements

This master thesis marks the end of my Environmental Engineering studies at LTH as well as it contributes to the very exciting X-band radar project and Future City Flow project. I would first like to thank Nicholas South with colleagues at VA SYD for the opportunity to be part of the X-band radar project during the summer and autumn 2018, which led to this thesis project and which have given me experiences of great value. I would also like to thank my supervisor at LTH, Magnus Persson for your support during the project. Further, I would like to thank DHI for the MIKE URBAN student licence and for providing me with great supervision – thank you Steve Berggren-Clausen for the interesting discussions and invaluable help with everything concerning the modelling part of this project.

And last but not least, many thanks to my family for the care and support when I spent the days stuck by the computer. I love you!

Abstract

Radar has been used since the 1940's to measure and monitor precipitation. In recent years the X-band radar has emerged as a tool to improve the input data to rainfall-runoff modelling within Urban catchments thanks to its high spatial and temporal resolution compared to other radars used for precipitation measurements. An X-band radar with a temporal resolution of one minute and a spatial resolution of 500 by 500 meters was installed in a pilot project run by VA SYD and LTH, ten kilometres east of Lund in the southernmost Sweden during July and August 2018. Although July 2018 proved to be one of the driest in Swedish history, August offered a handful of rain events of various intensity and duration. In this master thesis project these data were used as input data to a MIKE urban wastewater pipe system model over Lund, developed for a future real time monitoring and control of the inlet flow to Källby WWTP in southern Lund. The goal of the study was to conclude whether the X-band radar data could provide acceptable flow predictions compared to the measured values of the same period. As a reference, the model was also run with rain gauge data. The results showed that the X-band radar data can capture flow peaks that are missed by the rain gauge due to the spatial distribution of the rainfall, that dense rainfall above the radar itself may attenuate the signal enough to make the radar data largely underestimate the flow and that after low intensity rainfalls the radar data simulated flow peak occurs earlier than the measured. Another observation was that bias adjustment of the radar is needed. Overall, the radar has a potential to improve the modelling and to provide the data needed for real time smart control – if proper bias adjustment is obtained and the risk of underestimated flows after a heavy rain is minimized.

Sammanfattning på svenska

Radar har använts sedan 1940-talet för att mäta och övervaka nederbörd. Under de senaste åren har X-bandradarn visat sig vara ett verktyg som kan förbättra indata till avrinningsmodellering inom urbana avrinningsområden. Detta tack vare sin höga upplösning i tid och rum jämfört med andra radarer som används vid nederbördsmätning. En X-bandradar med en tidslig upplösning på en minut och rumslig upplösning på 500 x 500 meter placerades i Dalby, 10 km öster om Lund, inom ramen för ett pilotprojekt lett av VA SYD och LTH under juli och augusti 2018. Även om juli 2018 visade sig vara en av Sveriges torraste julimånader, bjöd augusti på en handfull regntillfällen av varierande intensitet och varaktighet. I detta examensarbete användes dessa regndata som indata till en MIKE urban spillvattenmodell över Lund, utvecklad för en framtida realtidsstyrning och -kontroll av inflödet till Källby reningsverk i södra Lund. Studiens mål var att dra slutsatser om huruvida X-band radardatan skulle kunna ge acceptabla flödesprognoser jämfört med uppmätta flöden under samma period. Som jämförelse kördes modellen även med regnmätardata. Resultaten visade att X-bandradadatan kan fånga flödestoppar som missas med regnmätardata på grund av regnets rumsliga utbredning; att kraftiga regn ovanför själva radarn kan försvaga strålen tillräckligt mycket för att radarn ska underskatta nederbördsmängden och att efter lågintensiva regnhändelser simuleras flödestopparna för tidigt med radardata jämfört med uppmätt mätserie. En annan observation var att biasjustering av radardatan behövs. Generellt kan studiens resultat sammanfattas med att radarn har potential att förbättra modelleringen och producera de data som behövs för en realtidsstyrning – om en passande biasjustering appliceras och risken för underskattade flöden efter kraftiga regn minimeras.

Table of Contents

Acknowledgements iii
Abstract v
Sammanfattning på svenska vii
Words and expressions 1
1. Introduction 3
1.1. Background 3
1.2. The X-band weather radar project 4
1.3. Future City Flow 4
1.4. Aims and objectives 5
1.5. Delimitations 5
1.6. Methodology description 5
2. Literature study 7
2.1. Sewage systems 7
2.2. Measure and estimate precipitation 11
2.3. Flow modelling in MIKE URBAN 17
2.4. Smart control 19
2.5. Nowcasting 21
3. Data collection and preparation 23
3.1. Raw data collection 23
3.2. Preparing data for MIKE URBAN 27
4. Modelling process 37
4.1. Description of the MIKE URBAN Lund model 37
4.2. Runoff simulation 40
4.3. Network simulation 41
4.4. Statistical analysis 41
5. Results and analysis 43
5.1. Overview 43
5.2. Rain gauge data 46
5.3. X-band radar data 48

5.4. Comparative analysis of highlighted events 52
6. Discussion 57
6.1. X-band radar data as input data 57
6.2. Modelling 60
6.3. Further questions 61
7. Conclusions 63
8. References 65
9. Appendix 71

Words and expressions

English	Explanation	Svenska
Climate adaptation	Measures to reduce vulnerability and increase resilience to climate change	*Klimatanpassning*
Combined pipe (system)	A sewage pipe (system) collecting both stormwater and wastewater in the same pipe	*Kombinerat system*
Combined sewer overflow (CSO)	When the capacity of a pipe carrying wastewater is full and water is directed to a receiving water	*Bräddning*
GIS	A system where geographical and physical data are analysed	*GIS*
MIKE URBAN	Modelling software used for simulations of, e.g. flows and pressures in pipe systems	*MIKE URBAN*
Model predictive control	Automatic control based on model predictions	*Modellbaserad kontroll*
Nowcasting	Weather forecasting on a short time scale, up to 2 h in advance	*"Nutidsprognos"*
Rain gauge	Instrument collecting raindrops for rainfall measurements	*Regnmätare*
Separate/duplicate pipe system	A sewage pipe (system) where stormwater and wastewater are collected in separate pipes	*Duplikat system*
Sewage water	Generic term including both wastewater and stormwater	*Avloppsvatten*
Stormwater	Surface water originating from precipitation	*Dagvatten*
Surface runoff	Stormwater that is not infiltrated or evaporated, flowing over a surface	*Ytavrinning*
Wastewater	Used water from households, businesses or industries	*Spillvatten*
Wastewater treatment plant (WWTP)	Facility where wastewater is treated	*Avloppsreningsverk (ARV)*

1. Introduction

This section begins with a brief background to the project and then introduces aims and objectives, delimitations and a methodology description, as well as a reading guide.

1.1. Background

Water is vital for life, although it may cause severe damage to both people and constructions if not taken care of properly. In the urban environment, sewage systems are needed to transport wastewater from households and industries as well as to drain off stormwater from streets and buildings. In the larger cities in Sweden, pipe networks for this purpose were first constructed in the end of the 19th century (Naturvårdsverket, 2018). Until the 1950's these pipe systems were mainly constructed as combined systems, where wastewater and stormwater are collected in the same pipe. Since then separate systems, where wastewater and stormwater are collected in separate pipes, are standard and today the Swedish pipe system consists of both combined and separate pipes (Svenskt Vatten, 2016).

During heavy rains or longer periods of rain, a combined sewer makes up a risk for both environment and health when the pipe capacity is reached. Sewage water may enter the basements, exposing people to contaminants. To reduce this risk, overflow structures are often constructed in the pipe system, directing the excess water into a stormwater pipe that is led without treatment to a waterbody. Also separate systems are subject to flooding with health risks; stormwater or groundwater may leak into the wastewater pipe and thus exceeding its capacity, causing water to flow backwards into basements (Svenskt Vatten, 2016). Densification of the urban environment is another important factor affecting the risk of flooding and combined sewer overflow (CSO), as previously permeable surfaces are made impermeable and more households are connected to the pipe network (Semadeni-Davies *et al.*, 2008).

The sewage system in the future will not only need to cope with an increased urban population, but probably also with increased stormwater loads. According to the Swedish Meteorological and Hydrological Institute (SMHI), it is likely that the number of days with heavy precipitation will increase with 5-15 days and that the maximum precipitation amount during 24 hours increases by 10-50 % towards the end of the 21st century compared to normal (1961-1990) (SMHI a, 2017; SMHI b, 2017). Cloudbursts and heavy rains are however not only a future risk. Several Swedish cities experienced unusually heavy precipitation events during the 2010's, with 2014 as an extreme year where the annual flooding costs more than tripled, reaching 900 MSEK. Several thousand flood damages were reported as well as a few life threatening situations (Salomonsson *et al.*, 2017).

Several Swedish municipalities are actively working on or planning for climate adaptation in their local communities, completing stormwater and wastewater strategies and preparing for increased precipitation intensities and volumes (Thörn, Ekholm and Nilsson, 2017). Lund municipality is no exception and their flooding plan establishes that new buildings should not increase the flood risk in the surrounding areas but on the contrary strive to improve stormwater management. They also state that physical land space as well as personnel shall be made available as needed to reach the goals to eliminate and minimize damage from heavy rains and cloudbursts (Lunds kommun and VA SYD, 2018). In a near future the wastewater treatment plant in southern Lund will be shut down and the wastewater will be transported to Malmö. Although a major part of the catchment is connected to separated sewage pipes it is still affected by rainfall and there is a wish to control the wastewater volumes that will be transported (discussion VA SYD, 2019).

1.2. The X-band weather radar project

An important characteristic of cloudbursts is the difficulty to predict them, as they are generally caused by chaotic atmospheric conditions that are difficult to represent in a model. One possible part of the solution is the so-called X-band radar. It operates with a high temporal and spatial resolution, thus being able to provide detailed input information to the weather models (Hernebring and Mårtensson, 2013). Several studies and full-scale tests have been carried out on the topic of predicting cloudbursts and heavy rains with the use of X-band radar (e.g. CASA, no date; EnviDan, no date; RainGain, 2012; Goormans and Willems, 2013) and in 2018 the technique was first tested in Sweden, with an X-band radar installed east of Lund. This test period provided promising results, indicating that high-resolution radar data could become an important tool in the work towards decreased flood risk after heavy precipitation (South *et al.*, 2019).

1.3. Future City Flow

Future City Flow (FCF) is a Swedish project aiming to introduce modern decision support techniques to existing pipe systems. The goal is to develop a model predictive control tool, which can be used to mitigate or decrease flooding and combined sewer overflow. The project is a collaboration between industry, public water and wastewater organisations as well as academia and spans from 2017 to 2019, partially financed by Vinnova (Sweden's innovation agency) (Sweden Water Research, no date). Lund is one of the studied cities, and a MIKE urban wastewater model has been created with the purpose of a future real time control in the city's sewage system. By studying how this model behaves with X-band

radar data, this master thesis creates a link between FCF and the X-band weather radar project.

1.4. Aims and objectives

The purpose of this master thesis was to evaluate precipitation data from a local X-band weather radar as input to a MIKE urban model compared to classic rain gauge precipitation data. This in order to investigate if the accuracy of downstream flow estimations at the inlet to Källby WWTP may be improved, and thus if the output information is accurate enough to be used in an online flow control.

The aim is to conclude if the X-band radar data provide acceptable flow predictions at the inlet of Källby wastewater treatment plant.

The following questions formed the base for the thesis work:

- To what extent is bias adjustment of the raw radar data needed?
- Can X-band radar data improve the results in hydrological modelling with MIKE urban, compared to rain gauge data?
- What potential is there for X-band radar data in sewage modelling in Lund?

1.5. Delimitations

This thesis project was limited to input data during the X-band radar project time, lasting from July to September 2018. Furthermore, the radar was not site-specifically calibrated during this time, meaning that there might be large variations in the registered radar data compared to the characteristics of the real precipitation event. It was also assumed that the rain gauge measurements were a correct representation of the rain events. The model and data used represent Lund and the catchment of Källby wastewater treatment plant, and the results are not directly applicable to other areas.

1.6. Methodology description

Below follows a brief description of the methods used during the thesis work.

1.6.1. Literature study

To map and study the current status of available techniques and knowledge of precipitation measurements and sewage system modelling for real time control, a literature study was made. The literature study together with a presentation of the X-band radar used in this project are found in chapter 2.

1.6.2. Data collection and preparation

The precipitation data used in this project were supplied by VA SYD and consist of rain gauge measurements as well as X-band weather radar data. The X-band radar data were bias adjusted according to factors determined in the parallel master thesis project *Applying X-band radar data in urban hydrology - Adjusting data for a neural network model, based on the pilot project in Dalby 2018* (Hedell and Kalm, 2019). Both data sets were finally stored as time series, where the radar data were connected to a specific sub catchment and the rain gauge data were assumed valid for the whole area. These procedures are found in chapter 3.

1.6.3. Modelling using MIKE URBAN

With base in the precipitation data, a runoff simulation was performed with each data set. These results then formed the boundary condition for a network flow simulation, where the output results showed simulated inflow to Källby WWTP. The modelling procedure together with an introduction to the model are found in chapter 4.

1.6.4. Analysis and discussion of results

The results are first presented separately (depending on input data type: rain gauge data or radar data) and then analyzed and compared to each other. Observations from the analysis formed the base for the discussion. Results and analysis are presented in chapter 5, discussion in chapter 6 and conclusion in chapter 7.

2. Literature study

This section covers the background theory leading to this project: after an introduction to the Swedish sewage system, rainfall measurement with rain gauge and radar are presented followed by flow modelling and a description of MIKE urban, which was the modelling software used in this project. Finally, smart control and nowcasting connected to sewage systems are introduced.

2.1. Sewage systems

The sewage system is essential for the water management of a city, and below follows a general introduction together with specifics on Lund sewage system as well as future challenges and possibilities.

2.1.1. Current situation

As mentioned in section 1.1, the Swedish sewage system has undergone a development from the late 19th century's combined, untreated systems to duplicate systems where wastewater is treated and stormwater is (to various extents) detained on the surface before it is directed to a receiving water. Figure 1 shows a schematic illustration of this development, going from A to F, where D-F are present in various combinations today, although combinations of D and E are the most common.

A. No sewage system
B. Combined system leading the water to nearest water course
C. Extending the combined pipe, leading it further away and thus moving the pollution further away
D. Combined pipes leading to a treatment plant but with the possibility of directing untreated overflow to a nearby watercourse
E. Duplicate system where only wastewater is treated, and stormwater is directly led to a watercourse
F. Duplicate system where stormwater is detained and completely or partially directed via above-ground open systems, enabling some pollution removal before it enters a watercourse (Sörensen, 2018).

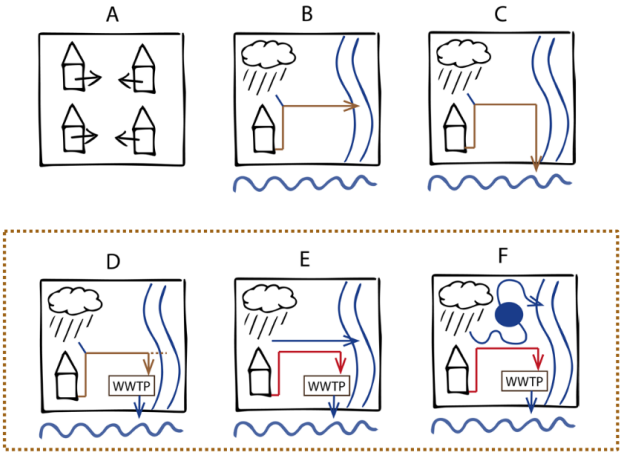

Figure 1. Schematic illustration of the development om Swedish sewage systems from the 19th century until today. Image D, E and F represent the systems found in use today. Image source: Sörensen, 2018.

Although many older pipes have been renewed, approximately 13 % of the total Swedish municipal sewage water is still transported in combined systems. Misconnections where stormwater enter the wastewater pipes (and vice versa) as well as leakage into wastewater pipes from, for example, stormwater and groundwater are also known problems that contribute to an increased risk of damming, flooding and release of untreated wastewater in existing pipe systems (Svenskt Vatten, 2016). As renewals, expansions and development come with gradual changes on the pipe systems, a system is often not either separated or combined, but a combination, see Table 1 for definition (VA SYD, 2018).

Table 1. Definition of existing pipe system types (VA SYD, 2018).

Type	Definition
Duplicate/separate system	Stormwater and wastewater are separated. Only wastewater is transported to a treatment plant.
Non complete duplicate system	Duplicate system where wastewater pipes are affected by combined pipes.
Combined system	Wastewater and stormwater are transported in the same pipe to a treatment plant.

2.1.2. Combined Sewer Overflow (CSO) and flooding

In Sweden each municipality is responsible for its pipe systems, either directly or through collaboration with other municipalities. They are, amongst other things, responsible for handling the stormwater to reduce flooding. This responsibility does only include stormwater generated by a rain with a statistical return period of less than 10 years (Svenskt Vatten, 2016). Since combined sewer pipes collect

both wastewater and stormwater, they are naturally more sensitive to high precipitation than separate wastewater pipes. During heavy rain events the capacity of these pipes, and possibly also of the treatment plant to which they transport the water, may be exceeded and untreated water is released untreated into a stormwater pipe or a nearby waterbody. This is defined as combined sewer overflow (CSO) and may have both short term and long term effects on the waterbody, where smaller receiving waters in general are more sensitive than larger (Naturvårdsverket, 1993).

Separated wastewater pipes may also be affected by precipitation. Misconnections (where stormwater is connected to wastewater pipes), damaged pipes and older drainage connections are examples that may cause stormwater to enter the wastewater pipe. This is defined as additional water and causes problems such as flooding or excess CSO since the capacity of neither wastewater pipe nor treatment plant is dimensioned to handle this additional water (Lundblad and Backö, 2012).

2.1.3. Prospects and possibilities

As described in section 2.1.1 the Swedish sewage system has been built and developed since the late 19th century. Large expansions were made in the 1950's to 1990's, and according to a study by Malm and Svensson (2011) as many as 50 % of the existing sewage pipes were constructed before 1972. The same study also concluded that the renewal rate of the older pipes needs to increase in order to meet the demands of a well-functioning sewage system, considering densification and activity changes of urban areas as well as the normal degradation due to age.

Climate change is expected to affect the precipitation patterns and thus increasing the need for a well-functioning sewage system. According to the Swedish Meteorological and Hydrological Institute (SMHI), it is likely that there will be 5-15 more days with heavy precipitation (> 10 mm / day) in the end of the 21st century, compared to a reference period of 1961-1990 (SMHI a, 2017). Likewise, the maximum precipitation amounts during 24 hours are expected to be 10-50 % larger than during the reference period 1961-1990 (SMHI b, 2017).

The concept of blue-green infrastructure as a stormwater management tool is a complementary strategy to pipe systems. These blue-green solutions use natural or artificial structures, often involving vegetation, and strive to collect stormwater in areas designed to detain and infiltrate excessive volumes (O'Donnell, Lamond and Thorne, 2017). The areas should preferably be multi-functional and during drier conditions function as parks, school yards or other publicly accessible areas (eg. O'Donnell, Lamond and Thorne, 2017; Lunds kommun and VA SYD, 2018;

Sörensen, 2018). With the proper design and terrain elevation analysis, blue-green solutions can mitigate local pluvial flooding and combined sewer overflow (Haghighatafshar *et al.*, 2018).

In dense urban areas, above-ground solutions are not the only complementary tool to collect and detain stormwater runoff. Since the 1990's there has been a future vision of a smarter pipe system volume control to reduce CSO. The general idea is to use the existing pipe volumes in an efficient way and thus detain water within the system (Wennberg, Nordlander and Hernebring, 2017). This type of setting was tested in Copenhagen around 2010 and a model predictive control tool was developed and fed with radar data. Offline tests were performed on three different catchments within Copenhagen, showing that overflow to some extent could be completely avoided or at least directed to less sensitive receiving waters if the systems were automatically controlled (Jørgensen *et al.*, 2012). As mentioned in the introduction section 1.2, the Swedish research project Future City Flow is aiming to develop a similar tool, which is why the MIKE urban model over Lund used in this project was developed. This concept of model predictive control is further described in section 2.4.

2.1.4. Lund

Lund is a growing city, with approximately 91 000 inhabitants in 2017 after a net increase of around 8 600 people during 2010-2017 (SCB, 2018). Densification is highlighted as an important strategy to increase the number of housing areas in the city to meet this population growth (Lunds kommun, 2016) and it is therefore important to renew and improve the pipe system at a high pace (VA SYD, 2018). In Lund, VA SYD is the public water organisation responsible for this renewal and improvement, keeping stormwater drainage safe for both people and environment (VA SYD, 2019). The wastewater from Lund city together with the wastewater from Dalby, Veberöd, Genarp and Stångby is directed to Källby WWTP in southern Lund. According to long-term plans however, this treatment plant will be shut down and the water transported to Sjölunda WWTP in Malmö. The main purpose of a future version of the model used this project will then be to estimate and control the flow to and from an equalization basin before transportation to Malmö (discussion VA SYD, 2019).

In general, the city has a duplicate sewage system, except for the older and central parts where just over 80 % of the pipes are combined, compared to around 10 % of the city's total sewage pipe length. Figure 2 shows the approximate areas connected to separate respectively combined pipes. This percentage of combined pipes, in combination with a prominent sloping topography generally provides a good base for a well-functioning sewage system. However, additional water entering the sewage pipes leading to Källby WWTP in southern Lund constitutes both a flood risk and an environmental issue (VA SYD, 2018). Stormwater and CSO from Lund city are directed to Höje creek (VA SYD, 2018), located south of the city and flowing west to meet Öresund (highlighted in Figure 2). The water course is classified as sensitive and eutrophicated, with poor ecological status (VISS, 2018).

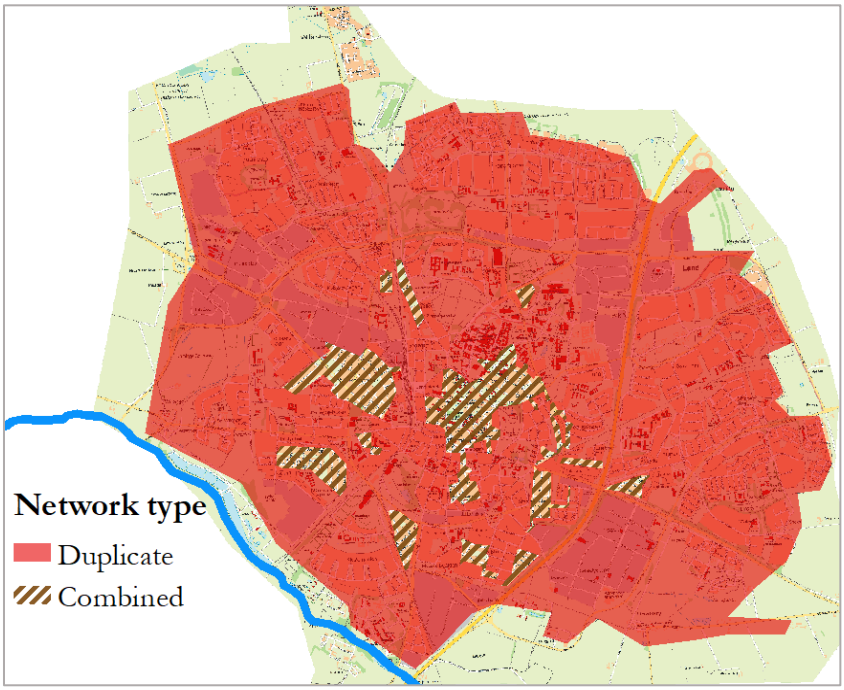

Figure 2. Map over Lund city, where (mainly central) areas connected to combined pipes are shown in brown. Höje creek is highlighted with blue in the south west.

2.2. Measure and estimate precipitation

There are various techniques available to measure precipitation. Rain gauges have been used and developed for centuries and today a variety of models and techniques are used; both with manual and automatic operation (SMHI a, 2018). Radars of different types for weather observation and measurements were first

used in the 1940's, with large developments since then (WMO, 2014). Today satellites may also be used to estimate precipitation (Shroder, 2016).

In urban state of the art hydrological modelling, point-measured rainfalls from rain gauges are commonly used as input data. Due to the variation in spatial distribution of – especially high intensity – rainfalls, the assumption that a few rain gauges can represent an entire catchment is beginning to be questioned. Therefore, the use of high-resolution weather radars has become more common, providing a possible compliment to the traditional rain gauge (Thorndahl *et al.*, 2017). When such a radar is installed however, rain gauges will still be needed for the initial and continuous calibration and bias-adjustment of the radar (e.g. Goormans and Willems, 2013; Borup *et al.*, 2016; Thorndahl *et al.*, 2017).

This section describes rainfall measurements techniques with rain gauges and radar.

2.2.1. Rain gauges

The basic principle for a rain gauge is that raindrops are collected in some type of container allowing for volume or weight measurements. For practical reasons, the traditional manual rain gauge only measures accumulated rain amounts; rain is collected in a storage device and the volume of water is manually emptied and logged together with the time and date. The more modern, automatic rain gauges are also capable of rainfall intensity measurements (SMHI a, 2018). The type of rain gauge used by VA SYD, and thereby the type of rain gauge used for this project, is the automatic so-called *tipping-bucket* rain gauge. Figure 4a shows an example of a tipping-bucket rain gauge, and Figure 4b shows a schematic illustration of a tipping-bucket rain gauge.

Figure 4a. Example of a tipping-bucket rain gauge. Image source: HyQuest Solutions.

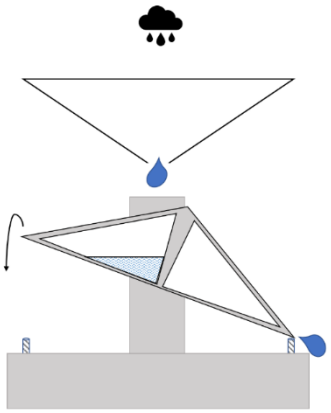

Figure 4b. Schematic illustration of the inside of a tipping-bucket rain gauge.

In this type of rain gauge, the raindrop is led down a funnel when it enters the gauge. The raindrop lands in a small bowl of determined volume and when this bowl is filled to a certain volume it tips over. As it tips down, the other (empty) bowl tips up; an electric pulse is generated and registered and the filled bowl is emptied. When the other bowl is full it tips over and the process is repeated (Mississippi WMO, 2017).

If the electrical pulse (the output data) is time-logged, the tipping-bucket rain gauge provides a good basis for intensity calculations. The tipping-bucket gauge is however not faultless and there is for example a risk that water evaporates from the bucket, especially during low-intensity rainfalls combined with warm temperatures (WMO, 2014). Wind is another common source of error in the measurements and depending on the location and design of the rain gauge, the registered rain might be underestimated by approximately 20 % due to this. Despite this possibly large source of error, tipping-bucket rain gauges are still a cost-efficient and fairly accurate way of measuring rainfall (Pollock *et al.*, 2018).

2.2.2. Radar

Unlike rain gauge measurements, radar provides the user with continuous, integrated data in both time and space. There are various types of radars, specified for various types of measurements; radars with the purpose of detecting precipitation are designed primarily for this but it can detect other items within the range (i.e. birds, insects and planes). Basic principles for different types of radars are described below.

Radar characteristics

The radar precipitation data are not direct measurements like the data produced by rain gauges. Instead, rain rates are calculated based on a reflectivity factor (Nielsen, Thorndahl and Rasmussen, 2013). A rotating antenna emits electromagnetic pulses, where the frequency differs with the type of radar. When this pulse hits a target, a return signal with changed frequency is scattered in multiple directions – including back to the radar. This return signal (echo) is characterized by its amplitude, phase and propagation. The amplitude depends on the characteristics of the raindrops hit by the radar beam and is used to determine

a parameter called reflectivity-factor (Z). This reflectivity factor is then used in an empirically derived equation to calculate rainfall intensity (WMO, 2014).

Different types of radars have different technical specifications. The most common type for meteorological purposes is the C-band radar (Pedersen, 2009) and this is the type used by SMHI in both research and every-day forecasting (SMHI a, 2013). The radar producing data for this project is a so-called X-band radar (South *et al.*, 2019), a radar type which can estimate rain rates with a higher temporal and spatial resolution than the C-band radar. Two drawbacks of the X-band radar compared to the C-band radar is however a shorter range and higher beam attenuation (Thorndahl *et al.*, 2017). Table 2 contains typical characteristics on wavelength, resolution and range for X-band radars and C-band radars, respectively (Pedersen, 2009; WMO, 2014; Thorndahl *et al.*, 2017).

Table 2. Typical characteristics for X-band radars and C-band radars. Note that the values vary with models, settings and calibration.

	X-band	**C-band**
Wavelength	3 cm	5 cm
Temporal resolution	1 – 5 min	5 – 10 min
Spatial resolution	100 – 1 000 m	250 – 2 000 m
Observation range	60 km	240 km
Quantitative estimation range	30 - 60 km	100 – 130 km

To be able to use the high-resolution possibilities of the X-band radar, accurate calibration and bias adjustment are needed and various methods are applicable. The radar data are processed with different statistical correlations and correction factors generally based on rain gauge data (Nielsen, Thorndahl and Rasmussen, 2013). The rain gauge data are seen as the truth when calibrating and adjusting radar data, which may be problematic since the rain gauge point measurement in reality only mirrors its immediate surrounding (Borup *et al.*, 2016). Furthermore, if they should be used for calibration it is important to know the quality of these data. Clogging, mis-calibration (of the rain gauge) and errors in the data transmission are commonly occurring faults affecting the quality of the rain gauge data (Thorndahl *et al.*, 2017). The demand for reliable rain gauges and online-logging of rain gauge data is also highlighted as one important factor for the future use and improvement of the X-band weather radar placed in Dalby (South *et al.*, 2019)

X-band radar in urban applications

Radar precipitation measurements provide important information to urban hydrology. Offline-applications where radar is becoming important are for

example analyses of past flood events and modelling for future flood risks. With improved internet communications and radar resolutions, applications such as nowcasting and automatic control of large hydrological systems are becoming possible (Thorndahl *et al.*, 2017). Urban hydrology is to a large extent characterized by fast response times because of the low share of pervious infiltration areas compared to the hard, impervious areas where runoff water can flow relatively fast. Nowcasting and real-time modelling of urban areas therefore require a high temporal resolution of the input data. An urban area contains several sub-catchments, and if the model represents this level of detail, the input data also need to be of high spatial resolution (Pedersen, 2009). Another situation where high spatial resolution is useful is when detecting storms with a small geographic spreading that move fast. The X-band radar is becoming a widespread tool in urban hydrology with the possibility to meet these demands (Thorndahl *et al.*, 2017). For the radar to be an efficient tool however, calibration is needed (Nielsen, Thorndahl and Rasmussen, 2013).

As mentioned in the beginning of this section, two drawbacks of the X-band radar is its relatively short range and weakness for attenuation. One measure to decrease the effect of these drawbacks is to install several X-band radars within an overlapping range. By using online data management, the data from the individual radars are combined and the total data set is to some extent compensated for the short range and beam attenuation of the individual radar (Wang and Chandrasekar, 2010; Antonini *et al.*, 2017). Another method may be to combine the data from the X-band radar with the data from a C-band radar, also using online data management (Nielsen, Thorndahl and Rasmussen, 2014). However, both techniques require advanced data processing in order to sync the data properly (Wang and Chandrasekar, 2010; Nielsen, Thorndahl and Rasmussen, 2014; Antonini *et al.*, 2017).

Dalby X-band radar – a Swedish pilot project

In the beginning of July 2018 Sweden's first X-band radar for hydrological purposes was installed. It was placed on the top of Dalby water tower in Lund municipality (see Figure 5, the radar was located at the marker) within the scope of a pilot project conducted by VA SYD, Lund University, Sweden Water Research and SMHI. The project lasted for two months and in September 2018 the radar was dismantled (South *et al.*, 2019). In April 2019 the radar was

reinstalled on Dalby water tower – the pilot project led to Sweden's first permanent X-band radar for hydrological purposes.

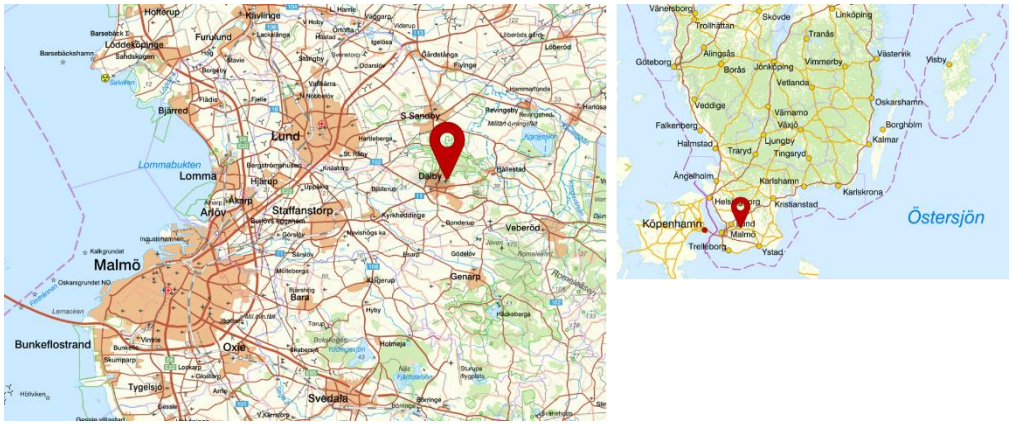

Figure 5. Location of the X-band weather radar used in this project.

The radar is a Furuno WR-2100 X-band radar, sending and receiving simultaneous horizontal and vertical pulses at a maximum antenna rotation of 16 resolutions per minute, which generates around 60 MB data per minute. The radar scans at different (adjustable) angles, where the sampling altitude increases with angle and distance from the radar. The data used in this thesis were collected at scan level 2, with an angle of 4 degrees. This means that the sampling altitude in Lund, approximately 10 km west of the radar, is almost 700 meters above ground. The maximum observation range is 60 km enabling monitoring over a large part of southern Scania (South *et al.*, 2019) – see Figure 6 for a snapshot from a rain event in August 2018. No calibration or bias adjustment was conducted according to the local conditions during the test period. However, a bias correction coefficient was developed with the mean field bias correction methodology within the scope of the master thesis *Applying X-band radar data in Urban hydrology – Adjusting data for a neural network model, based on the pilot project in Dalby 2018* (Hedell and Kalm, 2019). The bias correction was based on rain gauge data from several rain gauges in the VA SYD region and radar data from the grid cell surrounding the rain gauge. Table 3 shows the different coefficients determined for each rain gauge area as determined in the just mentioned thesis. The radar data used in this project were multiplied with the Lund coefficient (0.7293) as well as the median coefficient (0.2536), resulting in two radar data sets. The median was chosen before the mean in order to minimize the influence of the extreme values. Analysis and discussion around these coefficients are found in the above mentioned report.

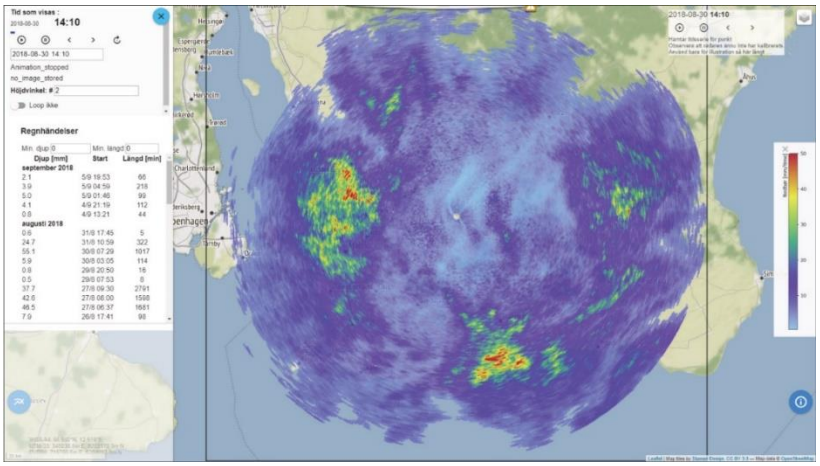

Figure 6. Snapshot from a rain event the 30th of August 2018, captured by the X-band radar in Dalby. The observation range covers large parts of southern and central Scania. Source: vasyd.informetics.se.

Table 3. Mean field bias correction coefficients determined in the master thesis TVVR 19/5004 (Hedell and Kalm, 2019).

Rain gauge	Bias correction factor
Åkarp	0.1425
Billinge	0.2944
Bulltofta	0.2799
Eslöv	0.2536
Hammars park	0.2437
Kungshult	0.2173
Löberöd	0.2619
Lund södra	0.7293
Marieholm	0.2324
Södra Sandby	0.1705
Turbinen	1.2057
Median	0.2536
Mean	0.3665

2.3. Flow modelling in MIKE URBAN

Modelling is the attempt to describe reality and flow modelling covers many different applications; modelling of future possible measures on the pipe system, re-analysis of flood events and near real-time flow predictions are some examples (Blomquist *et al.*, 2016). The hydrological model may range from pure statistical to physically based. A purely statistical model is dependent on large amounts of data to produce representative results, whereas a physically-based model (in theory) contains all physical data needed to represent the studied catchment without the need for long data series. In practice, most models are built using both statistical and physical elements in various proportions (Larsson, 2018).

This section describes the GIS-based modelling software MIKE urban, which was the model type used in this study. Specific details on the model used in this project is found in section 4.

2.3.1. Software

MIKE urban is a GIS-based hydrological modelling tool developed by the company DHI that includes geographical catchment characteristics as well as pipe network data. Two examples of important catchment characteristics are total surface area and average imperviousness, which both govern the amount and timing of the generated runoff. Important pipe network characteristics include network type (combined, wastewater or stormwater), pipe diameter and the slope between two connected manholes or other structures. Other valuable information includes for example if pipe leakage occurs as well as locations and characteristics of overflow structures, pumps and detention basins. While model data and characteristics are stored and constructed in MIKE urban using a geodatabase, the modelling computation is carried out by a built-in modelling engine. This solves a number of hydrological equations and relations to determine, for example, rainfall-runoff and pipe network flow (DHI a, 2017). Flows and levels for both single events and long-term effects can be modelled. To compute pipe network flows and levels, a primary modelling with rainfall input data computes the runoff generated. In a next step, the runoff result is used as a boundary condition to compute the pipe network flows and levels (DHI b, 2017). Figure 7 shows a schematic illustration of the process. To achieve a well-performing model, calibration and validation is needed. During this process, model results are visually and statistically compared to measured values. These measured values can for example be flow, water levels and velocity (DHI a, 2017).

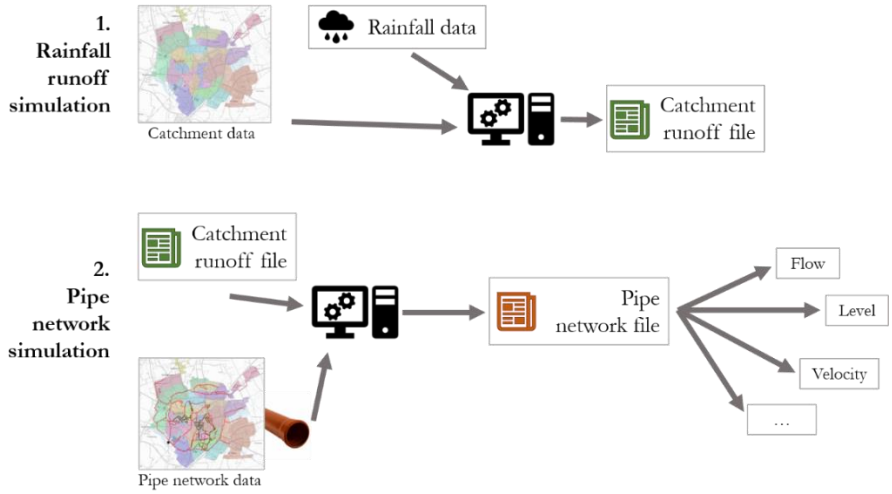

Figure 7. Schematic sketch of how pipe network flows are modelled in MIKE urban, where a rainfall runoff simulation is performed prior to a network flow simulation.

MIKE urban supports real time control (RTC) of sewage systems (DHI a, 2017), and was used for example in the large-scale RTC-pilot test METSAM on three wastewater treatment plant catchments in Copenhagen (Jørgensen *et al.*, 2012). In Sweden, DHI and VA SYD are two of the organisations involved in the previously introduced project Future City Flow (FCF) (Sweden Water Research, no date). The MIKE urban model used in this project was developed within the scope of FCF, with the intention to be used for future automatic control of Lund sewage system.

2.3.2. Data requirements

A precipitation boundary condition in MIKE urban should be in the time series format *.dfs0* or *.dfs2*. The former (e.g. rain gauge data) varies in time and is connected to specified catchments in the model. The latter (e.g. radar data) is a raster format and varies both in time and space. Depending on the purpose of the modelling, MIKE urban can be ran with either fictive or real rain events. Output data from the model may for example be water levels in basins and manholes, flows in the system and estimated CSO amounts (DHI b, 2017). In this project, discharge at the inlet to Källby WWTP was of interest.

2.4. Smart control

As previously mentioned in section 2.1, the use of control strategies represents one piece of the puzzle towards a more stable Urban sewage system. Real Time Control (RTC) is a widespread technique where a mathematical model is fed with live – real time – data from sensors within the system and then calculates the optimal setpoint for pump power, valve regulation etc. In urban water applications the model may for example be designed to minimize pollution levels in the water released from a wastewater treatment plant, to minimize overflow volumes or controlling inlet to treatment plans (Vanrolleghem, Benedetti and Meirlaen, 2005). The RTC technique in this field has been available and used since the 1970's, but unstable sensors as well as limited computational power and communication systems have hindered development and implementation. With today's improved technique and online communication, Model Predictive Control (MPC) is rising as a promising development of the RTC. This trend is reflected for example in the number of published scientific articles on the subject, which doubled 2013-2017 compared to 2008-2012 (Lund *et al.*, 2018). This section describes the concept of MPC and gives some examples of projects and sites using the technique. Figure 8 shows a schematic illustration of the difference and similarity between RTC and MPC.

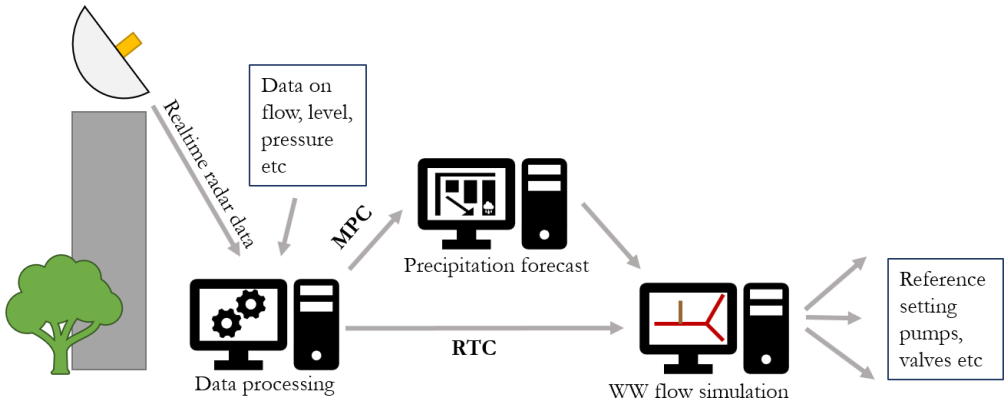

Figure 8. Schematic illustration of RTC vs MPC.

2.4.1. Model Predictive Control (MPC)

The model predictive control system uses forecasts to predict the input values to a mathematical model. A rainfall forecast instead of direct rainfall data is modelled to generate certain flows and levels in the sewage system, and these are then used to prepare the system for the next situation. It is a quite flexible system and functions for both large, complex, multi-variable systems as well as on a smaller and local scale and this is one of the reasons to why MPC is seen as a part of the solution in the work to prepare the sewage system for increased stormwater loads (Lund *et al.*, 2018). Compared to the alternatives of larger pipes and other physical modifications, this is often seen as a cost-efficient measure when investing and improving the sewage system (Vezzaro and Grum, 2014).

The MPC is generally performed with a discrete time step, meaning that the setpoints are continuously updated as new information is provided (Lund *et al.*, 2018) and this approach has been seen to decrease or avoid both flooding and CSO by controlling pumps and valves to better use upstream volumes that tend to be empty while such conditions are observed further downstream in the system (Thorndahl *et al.*, 2013). Even though a state of the art MPC control system is implemented, flooding and overflows are expected to happen when extreme rains occur. These are still both too unpredictable and too large for the control system to handle (Thorndahl *et al.*, 2013), although they could be used to produce warning alerts if flooding is unavoidable (Vezzaro and Grum, 2014).

When the rainfall forecast input data is of high spatial resolution, this makes it possible to use models that represent the heterogeneity of the urban catchment as these tend to be either too large or too complex to assume an equally distributed rainfall (Löwe *et al.*, 2014). An issue with detailed models is the increased computational time (Thorndahl *et al.*, 2013). However, practical

experiences have shown that simplified models where several sub catchments are lumped upstream a control point provide acceptable runoff simulation results (Löwe *et al.*, 2014).

2.4.2. Practical experiences

If the lack of adequate technical equipment was the traditional limiting factor, other factors are slowing the implementation today. In a review study from 2018, Lund *et al.* highlight a limited collaboration between the planners and operator and lack of trust amongst operational personnel as two important factors behind this, along with the uncertainty in the rain input data.

Directly related to this thesis project is Future City Flow, where academia and industry work together to develop a model predictive control tool. Real time data on for example flows, pressures and weather are fed into a model, which will then determine the short-term optimal conditions to reduce for example CSO, flooded pipes or costs for wastewater treatment. In the long term, the goal is that this tool will be an important support for the strategic city planning (Sweden Water Research, no date).

Across Denmark, a handful of wastewater treatment plants are operating with radar-based forecasts as part of the MPC optimized treatment control, with predictions of inlet flows and volumes (Krüger A/S, no date). Between 2010 and 2012 a pilot project similar to Future City Flow was carried out in Copenhagen, with the goal to develop real time technology that would be a cost-efficient tool and optimize the existing sewage systems. One important conclusion from the offline and online tests during the project was that runoff prognoses based on radar data are possible to successfully link to a control system over sewage system and sewage treatment plant. The sewage control system used pumps and valves to control and regulate the flow based on setpoints determined by model computations. One factor considered by the control system was the environmental cost of releasing CSO at the different overflow locations, where the most environmentally sensitive receiving waters brought the highest cost. It was then possible for the system to detain or redirect flows to decrease or avoid CSO to the most sensitive receiving waters (Jørgensen *et al.*, 2012).

2.5. Nowcasting

Most people are familiar to weather forecasts, which allow us to have an idea on the weather during a defined time frame. They are based on observations on various meteorological data such as wind, temperature, air pressure and humidity. These data are processed in physical models and the outcome is a possible weather scenario. The closer to "now" these forecasts get, the more they are based

on automatically reported data from weather stations and remote observations such as radar and lesser on the model results (SMHI c, 2017). Nowcasting is the term for very short forecasts, predicting the weather in the nearest couple of hours, that are primarily based on pure extrapolation of observed radar data (Thorndahl *et al.*, 2013).

SMHI uses a nowcast method called KNEP (short precipitation forecasts), that combines radar observations from the BALTRAD-network that covers the Baltic region with a meteorological model. It uses a weighted combination of observed and modelled data, such that for the shortest time scale, 90 % of the information is radar data and the rest is modelled data (SMHI e, 2018).

As mentioned in the previous section, urban control applications require detailed data and as the traditional forecasts are provided on a larger geographical scale than needed within a city, they are generally too rough for these online applications. Therefore, nowcasting with input from high-resolution radars (such as the X-band radar) are rising on the agenda, showing great potential (Thorndahl *et al.*, 2017). It has for example been shown that if several X-band radars are combined in a network and the data is used together with other meteorological data, they can significantly improve the accuracy of the nowcast (Antonini *et al.*, 2017).

An important drawback with nowcasts is that when they rely only on extrapolation of observations they tend to be accompanied with large uncertainties, which in turn affect the output from a model used in a control system (Vezzaro and Grum, 2014). Especially convective storms, often formed under chaotic circumstances and where precipitation may be unevenly distributed on the urban scale, has shown to be difficult to predict only with extrapolation. To decrease the uncertainties, radar data can be stochastically blended with numerical weather models. Despite these uncertainties, nowcasting still has a large potential in both model predictive control and urban flood warning systems (Thorndahl *et al.*, 2017).

3. Data collection and preparation

The precipitation boundary conditions used during the modelling were set according to a series of rain events that occurred during August 2018. The X-band radar test period lasted from the 3rd of July to the 11th of September, but near to no rain was registered in Lund in July. In September the rain fell after the test period had ended and the radar was dismantled. Figure 9 shows the accumulated monthly precipitation registered by two rain gauges in Lund during July and August 2018; one operated by SMHI and the other by VA SYD, compared to normal precipitation amounts (reference years 1961-1990). It is thus these scarce rain amounts in July that limit the actual data collection period to August.

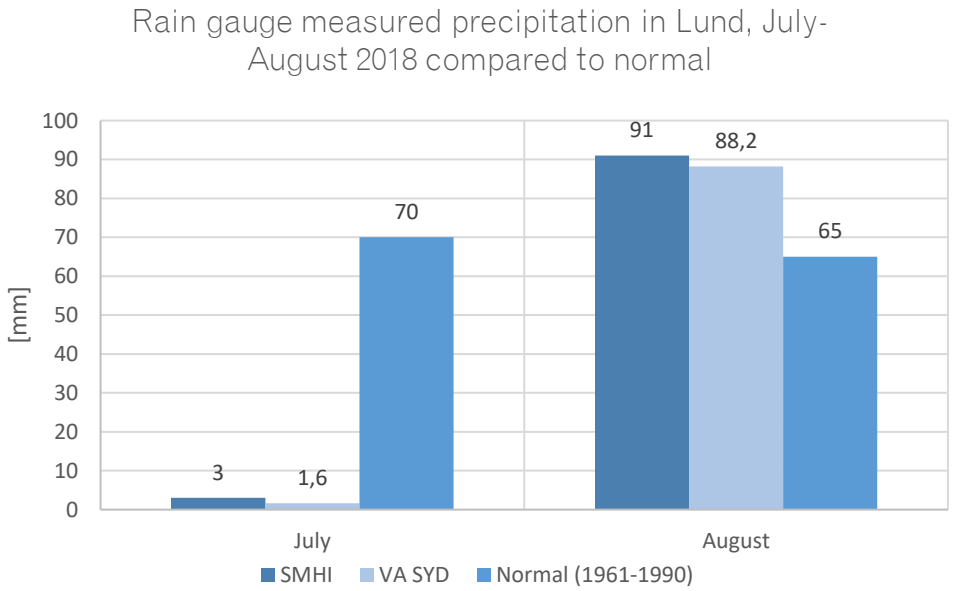

Figure 9. Accumulated precipitation amounts in Lund registered in two different rain gauges, July-September 2018 (SMHI b, 2018; SMHI c, 2018; SMHI d, 2018).

The following section describes the different rain events and the raw data collected as well as how it was bias-adjusted and arranged to the desired format needed in MIKE urban.

3.1. Raw data collection

Precipitation was measured by a tipping-bucket rain gauge and the X-band radar, flow was registered by a flow meter at the inlet of Källby WWTP. Rain gauge raw data as well as flow measurements were provided by VA SYD and the radar data were provided by VA SYD through a web tool developed by Informetics.

3.1.1. Rain gauge

During the study period VA SYD only had one operating rain gauge in Lund, located in the southern part (Figure 10). Figure 11 shows total daily accumulated rainfall in Lund during the test period as measured by this rain gauge in southern Lund. Lighter blue bars represent events with an assumed effect on the flow to Källby due to the larger volumes. Figure 12 shows an overview of the observed rain events, with accumulated rain volume over time. It is seen that different types of rains regarding temporal and spatial spreading, intensity and accumulated rain volume were observed.

Figure 10. Location of the rain gauge used for data collection.

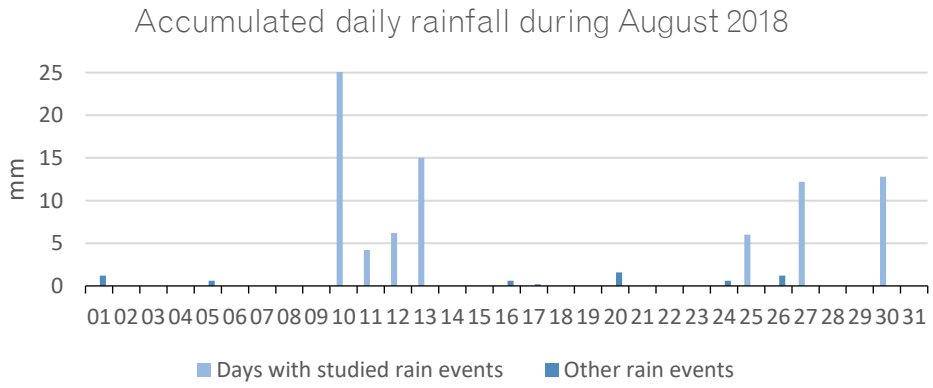

Figure 11. Accumulated daily rainfall during the radar test period, July-September 2018, as measured by a rain gauge in southern Lund.

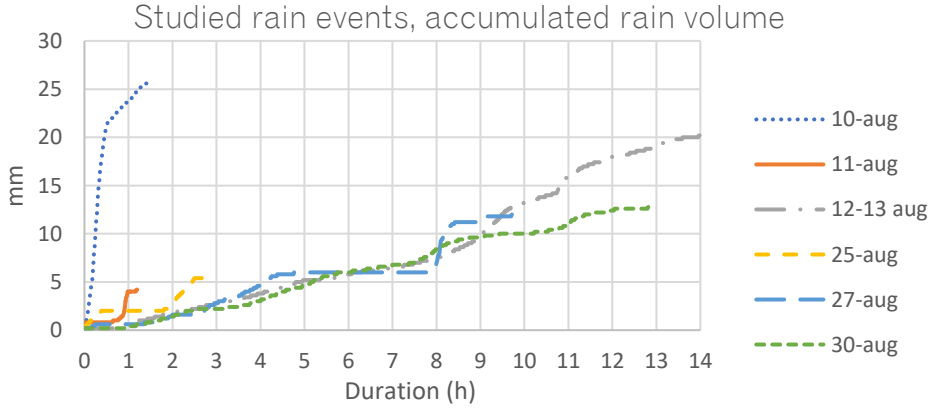

Figure 12. Accumulation over time for the studied rain events as measured by a rain gauge in southern Lund.

Below follows a brief description of these rain events:

Date	Description	Amount	Duration
Aug 10	The first precipitation in Lund after weeks of draught. High intensity rainfall.	26 mm	1.5 h
Aug 11	Local showers with varying intensity.	4 mm	1 h
Aug 12-13	Long lasting and light to moderate intensities.	20 mm	14 h
Aug 25	Local showers with varying intensity two events with a few hours' gap.	5.6 mm	3 h
Aug 27	Light intensity rainfall followed by higher intensity after a five hour's gap.	12 mm	9h 40 min
Aug 30	An event similar to the 12th-13th.	13 mm	12h 50 min

The tipping bucket rain gauge produced data pulses, where each pulse was time-logged (yyyy-mm-dd hh:mm:ss), representing 0.2 mm of rain. The data were exported to .txt files and Table 4 shows an example of the output data format.

Table 4. Example of the raw data output from the tipping bucket rain gauge.

Date, yyyy-mm-dd	Time, hh:mm:ss	[mm]
2018-08-11	21:17:12	0.2
2018-08-11	21:17:56	0.2
2018-08-11	21:29:34	0.2
2018-08-12	15:43:30	0.2
2018-08-12	15:50:55	0.2

3.1.2. X-band radar

Unlike the rain gauge, the radar produces spatially distributed precipitation data. For every time step a raster image is produced, where each grid cell of 500 by 500 meters contains the rain intensity of the minute that constitutes the time step. When the radar data were downloaded, one time series for one single cell during the whole period was downloaded at the time. This decreased the total amount of data that needed to be stored and processed, as these time series only contained data points when precipitation was registered and as only data from the areas of interest needed to be downloaded. The original raster data stored information also when no precipitation was measured, and for the whole 50 km radius area covered by the radar. The procedure of radar data collection is thoroughly described in section 3.2.2, as it was closely entwined with the procedure of data preparation before the modelling.

Noise and a blind spot

The Dalby X-band radar (circled in Figure 13) is blind in the area closest to it, which resulted in little or no data in several grid cells in Dalby. However, as seen in Appendix table 1 where all catchments are listed, the direct runoff from Dalby is not assumed to affect the wastewater flow as wastewater and stormwater are collected separately. Areas where stormwater do affect the wastewater flow are for example the central parts of Lund, and as seen in Figure 13 there are gaps in the data coverage also here. This is due to radar noise, which occurs when the radar registers false signals as rainfall (Figure 14). To eliminate this, the company

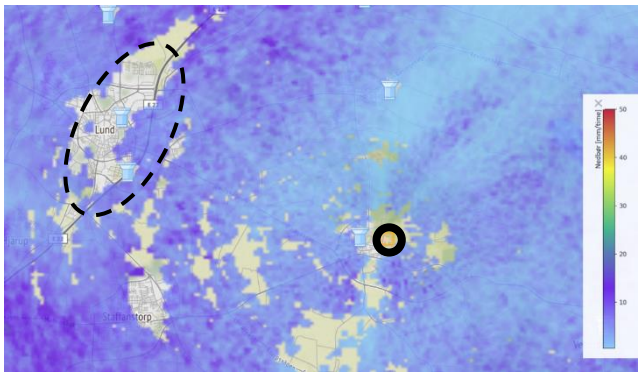

Figure 13. Snapshot from a rain event where the blind spot around the radar (circled) and the gaps from filtered noise over Lund are shown.

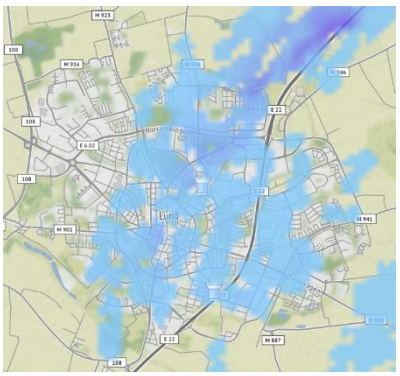

Figure 14. False radar rainfall signals during dry weather conditions.

who provided the radar data added a simple noise filter that automatically removed data points that suffer from noise. This resulted in the gaps seen over Lund in Figure 13. Effects of this are discussed in section 6.

Bias adjustment

The radar data were not bias adjusted when downloaded, and therefore multiplied with a bias correction factor that was introduced in section 2.2. In order to minimize the influence of the extreme values, the median bias correction factor was chosen. For comparison, the raw data set was also multiplied with the coefficient for Lund (see Table 5). Thus, the flow simulations were performed twice, with two different radar sets.

Table 5. The two bias correction coefficients used in this project.

Coefficient	Value
Lund	0.7293
Median	0.2536

3.1.3. Flow measurements

Inflow data to Källby WWTP were used to compare the corresponding estimated values from the model. The measured inflow during the test period is shown in Figure 15. A potentially limiting factor of this flow meter is that it has its maximum measuring range at 2.4 m^3/s.

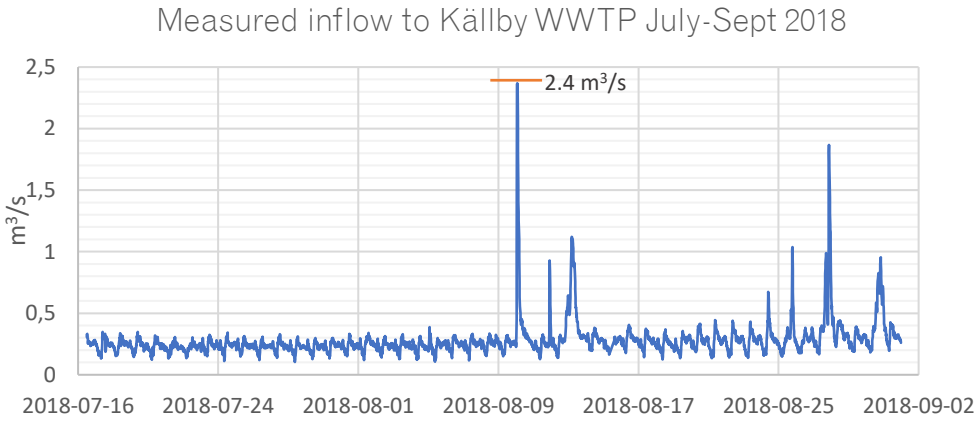

Figure 15. Measured inflows to Källby WWTP during July and August 2018.

3.2. Preparing data for MIKE URBAN

A precipitation boundary condition in MIKE urban should be in the time series format *.dfs0* or *.dfs2*. The former (e.g. rain gauge data) varies in time and is connected to specified catchments in the model. The latter (e.g. radar data) is a raster format and varies both in time and space (DHI b, 2017). In this project, the radar data were presented in raster format when downloading it and then converted to simple time series, weighted for each catchment. This section describes the procedure of preparing both rain gauge and radar data for MIKE urban.

3.2.1. Rain gauge

The raw data from the rain gauge in southern Lund were stored in a *.txt* file containing all rainfall events during July and August 2018, in the same structure as was shown in Table 4. This file was imported to MIKE urban, where the characteristics such as time format, measurement type and unit were specified, and then exported and saved in the MIKE urban time series format (*.dfs0*). Figure 16 shows an example of how this exported *.dfs0* file was structured after transformation from the .txt file. Since the raw data were presented as pulses of rain rather than intensity, the dfs0 file was structured likewise. One black line equals one registered pulse, meaning that several pulses in a short time (high intensity) is represented by several black lines in a short time.

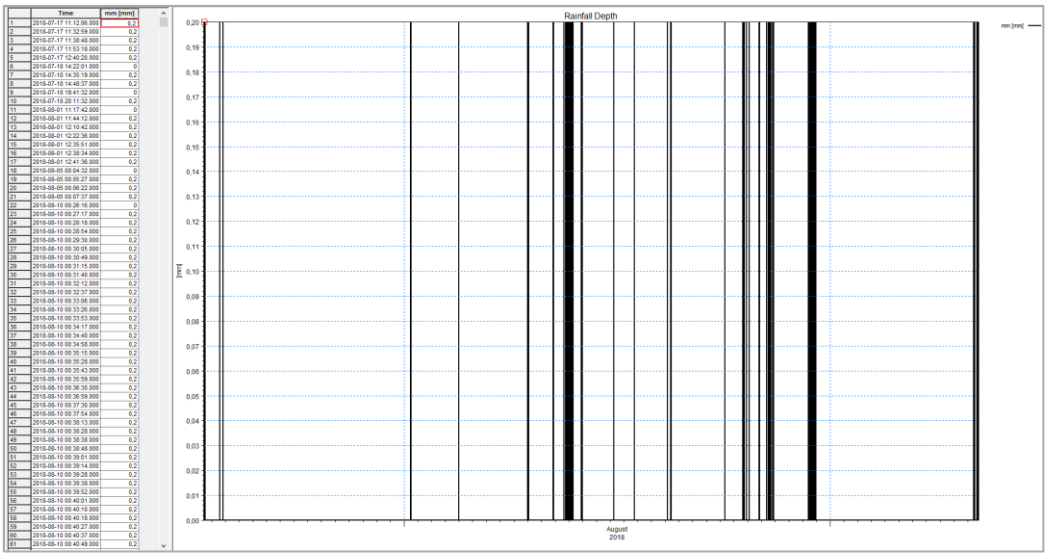

Figure 16. Example of the exported .dfs0 file, where each black line marks 0.2 mm registered rainfall.

3.2.2. Radar

The precipitation data produced by the radar were produced in a raster format, with one unique raster per time step (i.e., per minute). For the model to produce comparable results, the radar data needed to be in the *.dfs0* time series format. This required the radar data to be converted from its original gridded raster format with spatial reference to 29 time series (one for each catchment) similar to the one in Figure 16. To keep the spatial reference, each time series file then needed to be manually connected to the proper catchment before running a simulation in MIKE urban.

The gridded radar raster had a spatial cell resolution of 500 x 500 meters and naturally, the catchments and the grid cells were not overlapping perfectly. To get the representative data for each catchment, the influence of a raster cell on a

certain catchment was calculated based on how large part of the actual catchment the cell covered. Precipitation data for each grid cell were then downloaded from the external webtool. After the precipitation data for all contributing cells of a catchment were weighted, the total catchment precipitation was summarized.

The following steps give a more thorough description of the procedure.

1) Overlapping radar grid on catchments

To get an idea on how the radar raster was spatially related to the catchments, a raster file was placed on top of the catchment polygons in ArcMap. Based on this a grid was created, where each raster cell was mirrored by a square polygon. The catchment layer and grid cell layer were then combined using the "Union" tool in ArcMap, resulting in new polygons whose cell contours were the overlapping borders of the catchments and grid cells. Figure 17 shows an overview over Lund city where the different catchments are represented. Note how the polygon borders depend on both the grid cells and the catchment polygons.

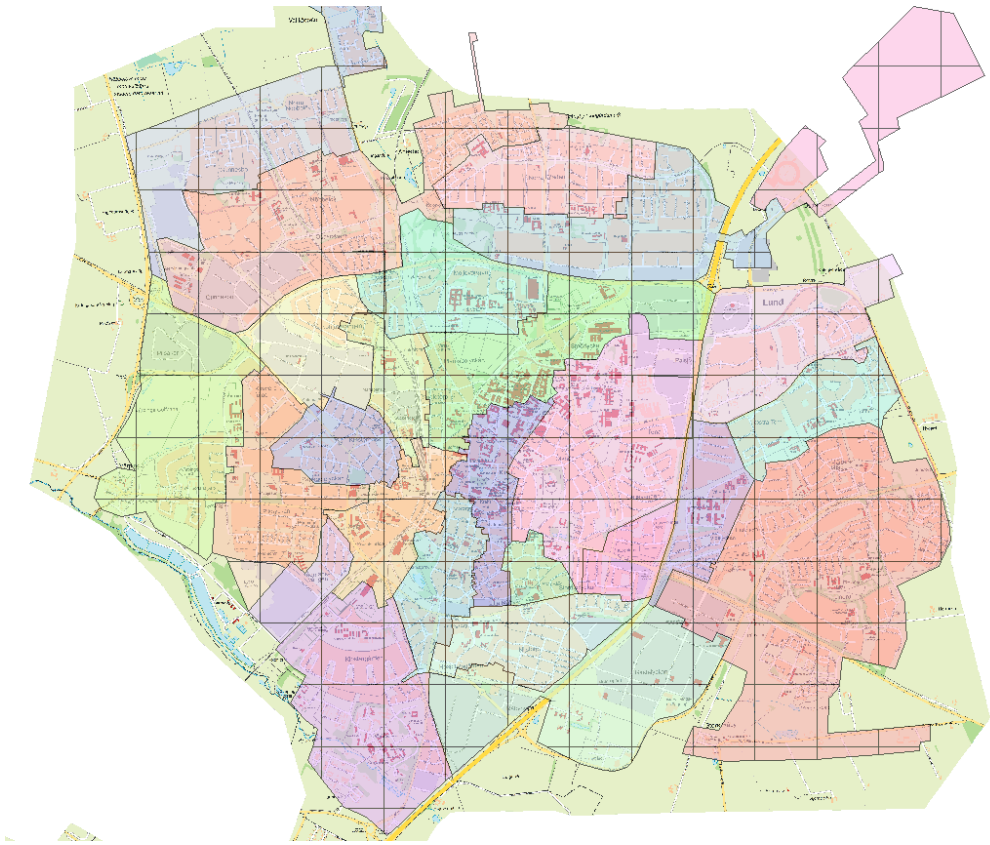

Figure 17. The catchment polygons combined with the grid cells.

2) Coverage factors

To be able to weigh the precipitation data in a grid cell to the correct proportion of a catchment, weighting factors were determined for each new polygon (see Figure 18). This was done in two steps:

a) How large part of the original grid cell is covered by the new polygon?

$$A = \frac{Polygon\ area}{Grid\ cell\ area}$$

b) How large part of the entire catchment does this represent?

$$B = \frac{Polygon\ area}{Catchment\ area}$$

A table with the corresponding *A* and *B* fractions were created, see Table 6. It is seen that for example Dalby catchment is larger than Vipeholm catchment, as a cell that is completely covered by Dalby catchment represents 7 % of the total catchment area, whereas the corresponding situation in Vipeholm means that the cell represents 41 % of the total catchment.

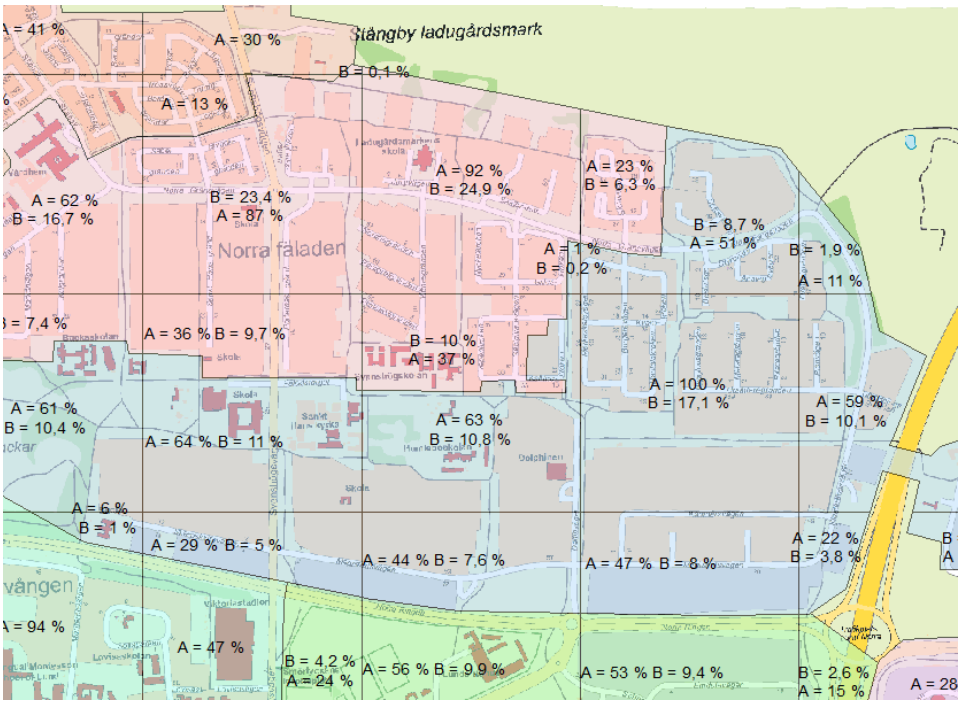

Figure 18. Illustration of the coverage fractions A and B, where A relates to how much of the grid cell that is covered and B to how much of the entire catchment that this represents.

Table 6. Example of weighting factors B based on how large part of a grid cell that was covered by the catchment (A), for four out of 29 catchments.

A	B – coverage in relation to total catchment area			
	6 Dalby	**28 Östra Torn N**	**25 Vipeholm**	**22 Pålsjö-Tuna**
100 %	0.07	0.21	0.41	0.12
90 %	0.06	0.19	0.37	0.11
80 %	0.05	0.17	0.33	0.10
75 %	0.05	0.16	0.31	0.09
70 %	0.05	0.15	0.29	0.08
60 %	0.04	0.13	0.25	0.07
50 %	0.03	0.11	0.21	0.06
40 %	0.03	0.08	0.16	0.05
30 %	0.02	0.06	0.12	0.04
25 %	0.02	0.05	0.10	0.03
20 %	0.01	0.04	0.08	0.02
15 %	0.01	0.03	0.06	0.02
10 %	0.01	0.02	0.04	0.01
5 %	0.00	0.01	0.02	0.01
1 %	0.00	0.00	0.00	0.00

3) Data collection

Via the web tool vasyd.informetics.se it was possible to download precipitation intensity data for single grid cells (Figure 19). Data for each grid cell included in the total Källby catchment area were downloaded and the grid cell was compared to the map in Figure 18 to estimate a proper fraction for cell coverage (A). Table 7 shows an example of how the data were structured for each grid cell.

In some areas there was a good geographical match between the web tool grid cell and the cell created in step 1, whereas other were more or less shifted and thus required a manual visual estimation of the catchment coverage (factor *A*). Possible reasons for, and consequences by, this are discussed in Discussion section.

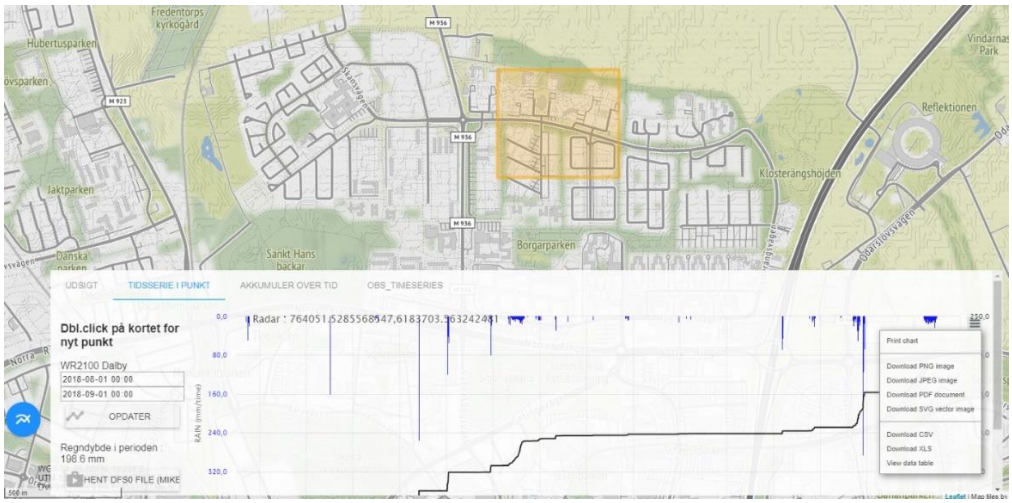

Figure 19. Screenshot from the web tool vasyd.informetics.se, from where the radar data were downloaded.

Table 7. Example of how the data were structured for each grid cell. The value in the catchment columns represent the A value; catchment 29 covered approximately 40 % of the cell.

DateTime	I (mm/h)	A 29 Östra Torn N	A 25 Vipeholm	A 22 Pålsjö - Tuna
2018-08-10 00:24	6.73064	0.4	0.3	0.3
2018-08-10 00:28	21.0775			
2018-08-10 00:29	183.708			
2018-08-10 00:30	61.4761			
2018-08-10 00:31	13.9493			

4) Completing the catchment time series

When data from all grid cells had been downloaded, intensity data together with the A factor for each catchment were collected in a separate MS Excel file. By using the conversion factor from Table 7, the corresponding *B* factor was noted. To check that all parts of the catchment were represented, the *B* factors were summarized. A sum equal to 1 was ideal and meant that all parts of the catchment area were properly included. Since much of the work in step 3 was done by manual visual comparison and was therefore not perfectly exact, a sum very close to 1 was also considered acceptable. If this was not the case the original data were checked again. *Table 8* shows two (out of six) catchment fractions from Vipeholm catchment, where the weighting factor B was multiplied with the rain intensity (mm/h).

Table 8. Example of catchment fractions for Vipeholm catchment, where the weight factor B was multiplied with the rain intensity.

Vipeholm, catchment fraction 1 and 2 of 6 with respective B factor

DateTime	I (mm/h)	A	B	$I_{weighted}$ (mm/h)	DateTime	I (mm/h)	A	B	$I_{weighted}$ (mm/h
2018-08-10 00:24	6.7	0.3	0.12	6.7*0.12	2018-08-10 00:27	87.9	0.2	0.08	87.9*0.08
2018-08-10 00:28	21.1			B*I	2018-08-10 00:28	173.2			B*I
2018-08-10 00:29	183.7				2018-08-10 00:29	62.3			
2018-08-10 00:30	61.5				2018-08-10 00:30	42.2			
2018-08-10 00:31	13.9				2018-08-10 00:31	45.9			
2018-08-10 00:32	17.9				2018-08-10 00:32	58.6			
2018-08-10 00:37	87.7				2018-08-10 00:33	41.6			
2018-08-10 00:38	52.3				2018-08-10 00:34	43.4			

The weighted intensity data from each grid cell catchment polygon were then summarized for each time step into a complete time series. A data point with zero intensity was inserted at 2018-08-09 00:00 (first) and 2018-09-02 00:00 (last), to assure that all catchment time series were starting and ending on the same time. This because the MIKE urban simulation can only run during the smallest common time span for every time series files. The complete time series was then multiplied with the bias correction factors introduced in section 3.1; the median bias correction factor (0.2536) and the Lund bias correction factor (0.7293), resulting in two time series with identical time steps but different intensities for each catchment. An excerpt of the complete Vipeholm time series is found in Table 9 (continues on the next page).

Table 9. Complete time series for Vipeholm catchment. The left intensity column is multiplied with the median bias correction factor, and the right with the Lund bias correction factor. The table continues on the next page.

DateTime	I_{median} (mm/h)	DateTime	I_{Lund} (mm/h)
2018-08-09 00:00	0	2018-08-09 00:00	0
2018-08-10 00:21	0	2018-08-10 00:21	0
2018-08-10 00:24	0.5	2018-08-10 00:24	1.4
2018-08-10 00:27	5.2	2018-08-10 00:27	15.0
2018-08-10 00:28	37.8	2018-08-10 00:28	108.7
2018-08-10 00:29	34.3	2018-08-10 00:29	98.5
2018-08-10 00:30	9.2	2018-08-10 00:30	26.3

DateTime	I_{median} (mm/h)	DateTime	I_{Lund} (mm/h)
2018-08-10 00:31	5.1	2018-08-10 00:31	14.5
2018-08-10 00:32	6.4	2018-08-10 00:32	18.3
…	…	…	…
2018-08-30 23:00	0.1	2018-08-30 23:00	0.2
2018-08-30 23:01	0	2018-08-30 23:01	0
2018-09-02 00:00	0	2018-09-02 00:00	0

Each time series was stored as a .txt file and converted to a .dfs0 file in the same way that the rain gauge data were converted. Thus, there were two files for each catchment; one with the lower, median bias adjusted intensities and one with the higher, Lund bias adjusted intensities.

As described in section 3.1, the radar data were subject to noise over several of the central parts, causing variations in the amount of data available in these catchments. Figure 20 shows the locations of the three catchments receiving the least (Lilla Råby), highest (Papegojlyckan V) and median (Linero) accumulated rainfall amounts during August 2018, among the catchments that contribute to runoff in the modelled pipe system (those that have an imperviousness greater than zero in Appendix table 1). Figure 22 and Figure 21 show the minimum, median and maximum bias adjusted accumulated time series with radar data. For comparison the accumulated rain gauge time series was added to each figure, and the y-axes show the same interval (0-200 mm). All the median bias adjusted data

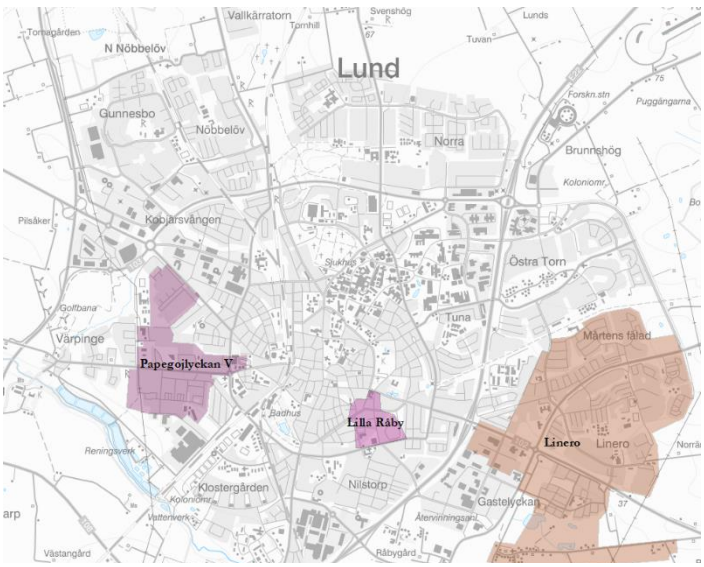

Figure 20. Geographic locations of catchemnts Papegojlyckan V (west), Lilla Råby (middle) and Linero (east).

sets show lower accumulated values than the rain gauge time series. The lowest time series (Lilla Råby) shows a total accumulated rainfall amount of less than 10 mm. In the Lund bias adjusted data set, the maximum accumulated value was almost a factor ten larger than for the minimum time series, while the median time series was close to the rain gauge accumulated time series. The number of registered datapoints were 102 in Lilla Råby (minimum), compared to 1941 datapoints in Papegojlyckan V (maximum). Each datapoint represents one minute of registered rainfall, and this shows the large spread in the completeness of the input data series.

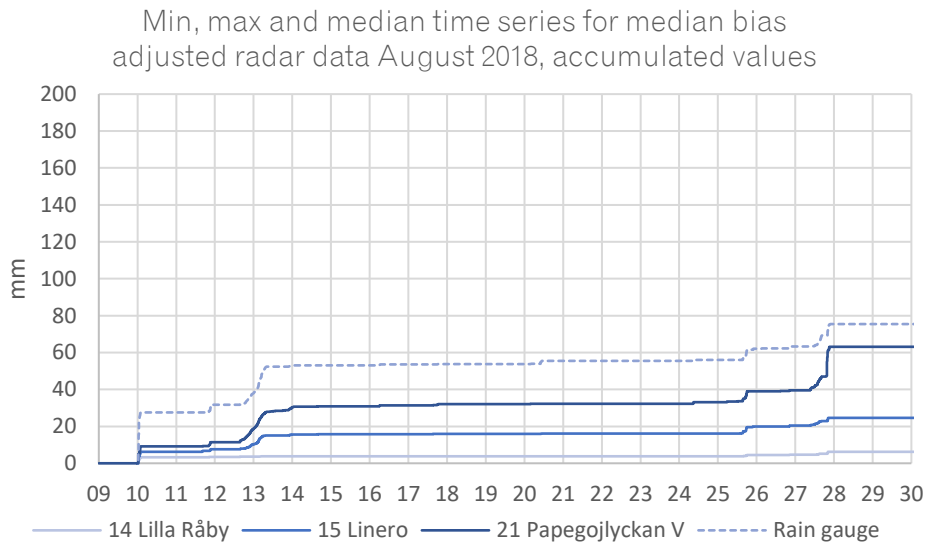

Figure 22. Median bias adjusted radar data time series compared to the rain gauge time series, accumulated values August 2018

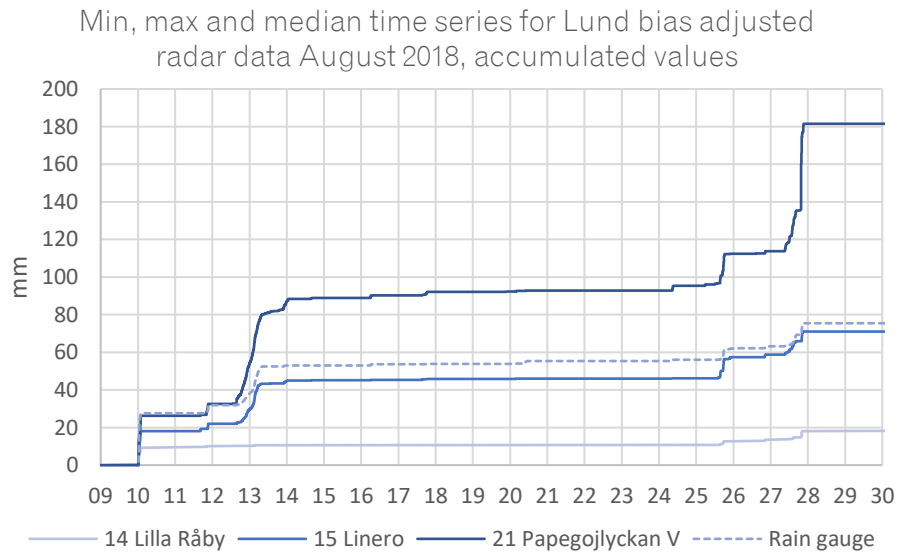

Figure 21. Lund bias adjusted radar data time series compared to the rain gauge time series, accumulated values August 2018

4. Modelling process

This section describes the model followed by the modelling procedure. The simulations were performed with the three data sets: rain gauge, median adjusted radar data and Lund adjusted radar data.

4.1. Description of the MIKE URBAN Lund model

This section describes the model used in this thesis project. It was constructed and calibrated by VA SYD and DHI and covers the areas contributing to the inflow to Källby WWTP in southern Lund. These areas include Lund city, Stångby Dalby, Veberöd and Genarp (southeast of Dalby). Lund, Stångby and Dalby are represented with catchments and thus directly affected by the precipitation input data, while Veberöd and Genarp are represented by a general cyclic inflow of wastewater. Figure 23 shows the catchment connected in the model, where the different colors represent the different subcatchments. Källby WWTP is marked with a black asterisk.

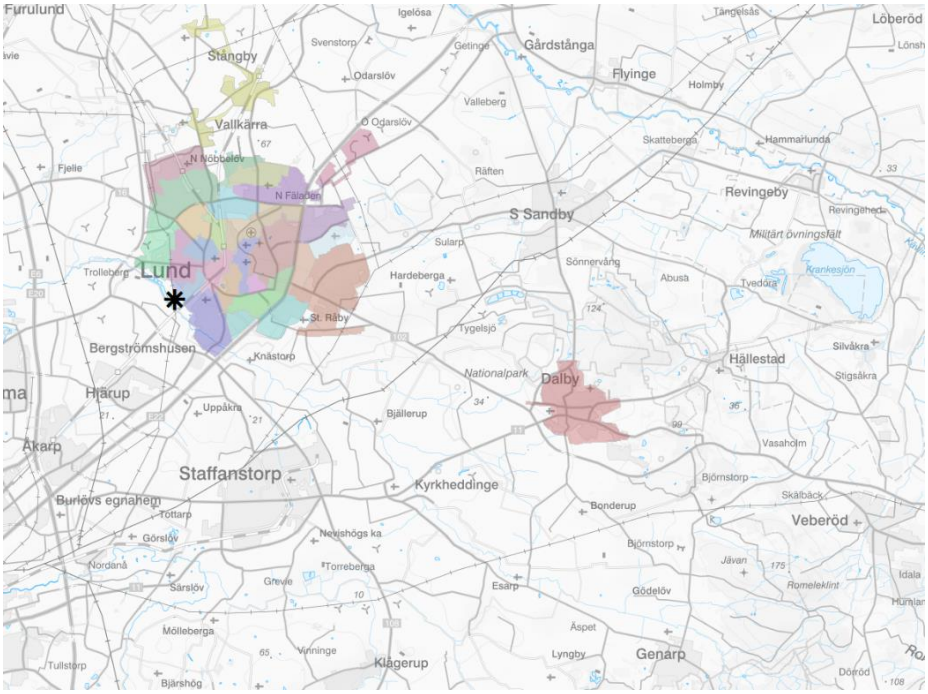

Figure 23. Overview over the catchment of Källby WWTP as described in the model.

4.1.1. Catchments

The total catchment area was divided into 29 subcatchments, of which 27 cover Lund city and the other two represent Stångby and Dalby. They range in size from 10 to 386 hectares and in imperviousness from 0 % to 30 %, according to Appendix table 1. The location of each catchment is shown in Appendix figure 1.

As this was a wastewater model it did not consider the separate stormwater flow only stormwater generated in areas connected to combined sewage pipes. The imperviousness is therefore a measurement of how much the catchment runoff contributed to the wastewater flow leading to Källby WWTP rather than how much runoff that is actually generated. The catchments denoted with zero imperviousness do generate runoff, although none of this was set to enter the wastewater pipe system. The flow was set as gravity-driven, and the catchment division was made according to which areas that transport the water to which basin and calibration measurement point. Each catchment was connected to a node (a manhole) where all the modelled runoff was assumed to enter the pipe system.

The catchments were set to produce runoff according to a time-area relationship, which is simple and fast due to its low data requirements. The relationship is based on how large share of the catchment area that contributes to runoff after a certain share of rainfall time (DHI c, 2017).

4.1.2. Pipe network

This model was designed for fast computations, enabling a future smart control of the total incoming flow to Källby (current WWTP, future equalization basin). Due to this the pipe network was simplified and represented by the larger main pipes. For the same reason pumps were excluded, except for the pumping station sending water from Dalby (including flows from Genarp and Veberöd) to Lund. This is likely to have a minor effect of the flow modelling, as the majority of the pipe flow is naturally driven by gravity.

Figure 24 shows Lund city as described in the model. Red pipes (dashed lines) are separated wastewater pipes, and brown pipes (filled lines) are combined. The thinner lines in in each catchment mark the node to which it was connected and thus where its runoff was assumed to enter the system. Källby WWTP is marked with a black asterisk in the southwestern part of the city. As described in section 2.1 a majority of the pipes are separated and as seen in Figure 24 the areas connected to combined pipes are found in the central, western and southern parts. Comparing this to Appendix table 1, it is seen that these areas have an imperviousness greater than 0. This means that in these areas, rainfall runoff has a short response time and a direct impact on the pipe network flow.

Eight combined sewer overflow (CSO) structures and three detention basins are represented, to which connected pipes are set to spill over when the flow capacity is reached. By implementing a smart control (see below), the use of these could possibly be used in a more efficient manner, decreasing the CSO. This is however not studied in this project.

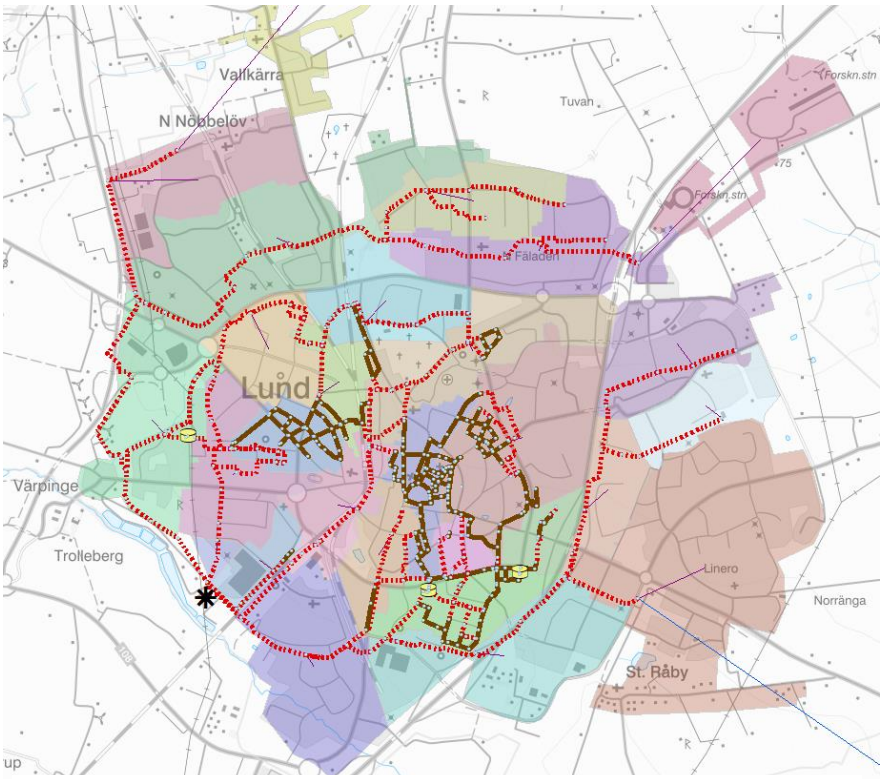

Figure 24. Overview over Lund city and the modelled pipe system. Red (dashed) lines represent separate wastewater pipes, brown (filled) lines represent combined pipes.

4.1.3. Calibration

Calibration of the model was not included in the scope of this master thesis. A rough calibration was performed by VA SYD and then it was fine tuned by DHI. It should also be said that the version used in this thesis project was not the final one, due to lack of time. Mainly, slow runoff such as leakage was not completely calibrated for. The fast runoff was however calibrated with respect to volume, timing and magnitude of flow peaks. To capture both slow runoff from drainage and leakage and fast runoff from directly connected surfaces these were calibrated separately. The most important factors to properly capture the slow runoff were constants controlling the runoff time and how the water was distributed between groundwater and different layers in the ground. Regarding the fast runoff the single most important factor was the runoff time from the connected areas, which primarily affects the timing and magnitude of the flow peaks. In order to capture

the correct volumes of water entering Källby WWTP, the size of the contributing areas was the most important factor.

The calibration period lasted between July and October 2018 (until February 2019 for some important catchments). This time period covers the study period for this thesis, a point discussed in section 6. Data for the calibration were collected by the permanent rain gauge in southern Lund (crossed circle in Figure 25), along with three temporary rain gauges (circles) and 17 flow meters (triangles) placed as shown in Figure 25. These temporary measurements were installed after the X-band radar in Dalby was dismantled, and their data were not directly included in this thesis project. In order to capture and calibrate for long term seasonal variations, the incoming wastewater flow was compared to flow data from 2014-2018 at Källby.

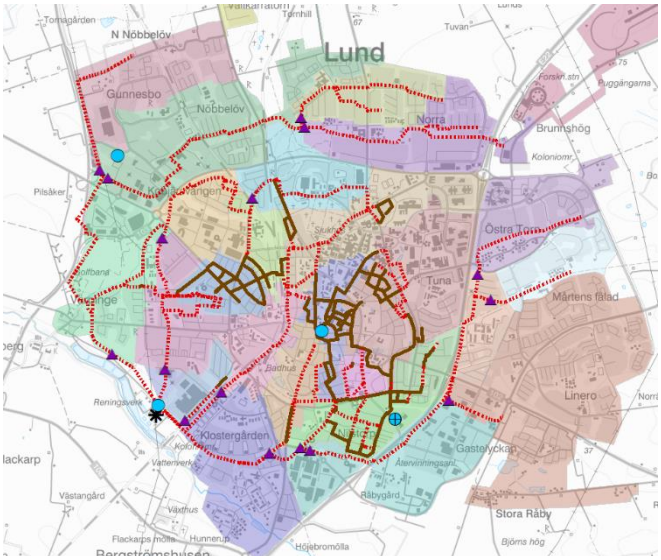

Figure 25. Rain gauges (circles) and flow meters (triangles) used for data collection during Autumn 2018.

4.2. Runoff simulation

As described in section 2, the first part of the MIKE urban flow modelling is a runoff simulation. Three parallel simulations covering August 2018 were performed; one simulation for each data set ((I) rain gauge, (II) median bias adjusted radar data and (III) Lund bias adjusted radar data). The rain gauge data were set to be representative for all 29 catchments, while the different radar data time series were set to be connected to its respective catchment. Each simulation produced a result file containing the generated runoff from each catchment. Again, since this model was designed to model wastewater flow, the modelled runoff was the runoff assumed to enter the wastewater system. A completely separated catchment was thus not producing any runoff in the simulation.

A background flow of average daily wastewater flows was applied in order to also capture the regular variations in the wastewater flow. Temperature and evaporation data were also applied.

4.3. Network simulation

The second step of the simulation was the network simulation; when the runoff generated in the previous step entered the pipe system. This simulation was heavier and more time- and data consuming than the runoff simulation. Therefore, the study period was modelled in three separate sections (with the three separate rain fall data sets):

1. August 9-14
2. August 15-20
3. August 21-31

The division was made to include the flow peaks in the measured inflow to Källby WWTP. August 1-8 was not included because neither significant rain nor flow peaks were registered during this time. The simulation was performed separately with the three data sets, thus resulting in nine different result files. These contained (amongst other things) simulated flows in the system. For each file, the discharge at the inlet to Källby WWTP was extracted and further analysed as presented in the Results and analysis section.

4.4. Statistical analysis

The simulated discharge from the wastewater pipe system to Källby WWTP was statistically analyzed with a built-in tool. For each of the nine result series, explained variance (R^2), peak error and volume error were calculated. See Table 10 for a brief description of the parameters (Persson, 2018).

Table 10. Description of the statistical parameters R^2, peak error and volume error (Persson, 2018).

Parameter	Description
Explained variance R^2	How closely the simulated data follows the measured flow pattern. Ranges from 0 to 1 where 1 represents a perfect match.
Peak error (%)	How well the simulated flow captures the measured peaks.
Volume error (%)	How well the simulated flow volume represents the measured flow volumes.

5. Results and analysis

This chapter presents the results from the simulations described in section 4. First, an overview of the complete study period (August 2018) is presented and the general trends are described. Then the results from the three sections are presented more thoroughly: first the simulated flows from the rain gauge data and then with the simulated flows from the X-band radar data with the median bias correction coefficient (0.2536) the Lund bias correction coefficient (0.7293). Lastly, five events are analysed and compared with respect to which of the three input data sets that were used.

5.1. Overview

An overview of the simulated and measured flows at the inlet of Källby WWTP in August 2018 (the studied period) is found in Figure 29. The daily variations in the wastewater flow are seen especially between the 14th and the 20th, when little or no rain was registered. Although the pipe system to a large extent is separated, there are still clear peaks occurring close in time to the precipitation events shown in section 3. It was also seen that the simulation results from the radar data corrected with the Lund bias coefficient generally produced higher flows compared to the two other data sets and compared to the measured flows.

5.1.1. Statistic correlations

The statistical analysis was run separately for each section. The average values for the explained variance R^2, the volume error and peak error are found in Table 11 and are graphically presented in Figure 26, Figure 27 and Figure 28.

Table 11. Average values for the complete testing period for R^2, volume error and peak error.

	Rain gauge	**Median bias factor**	**Lund bias factor**
R^2	0.73	0.64	0.65
Volume error	-4 %	1 %	0 %
Peak error	14 %	-38 %	5 %

The rain gauge data set shows an average correlation coefficient of 0.73, which is the highest of the three data sets. Looking at the average volume error, all three data sets show a volume error of less than 5 %. The average peak error shows that the rain gauge data set generally overestimates, while the median bias corrected radar data set generally underestimates. The Lund bias adjusted data set again show a low average error (5 %).

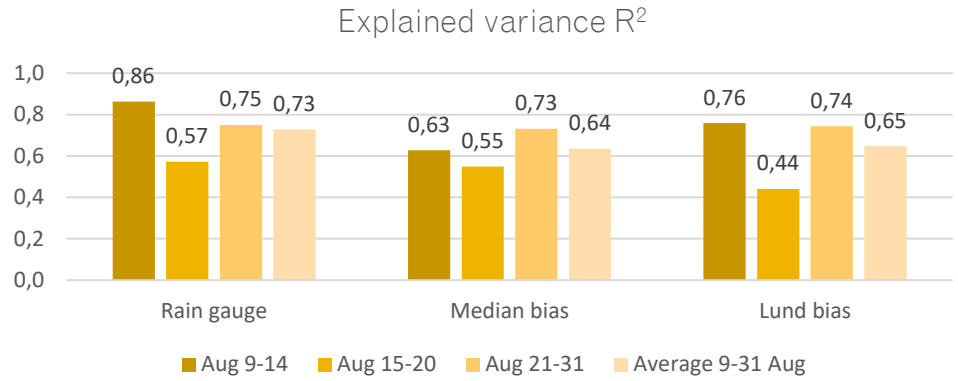

Figure 26. Explained variance (R2) for the different data sets, along with the average value.

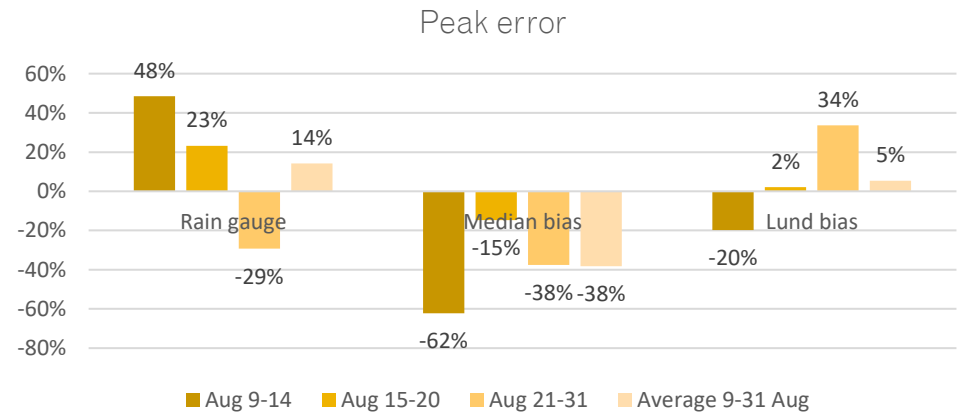

Figure 27. Peak error for the different data sets, along with the average value.

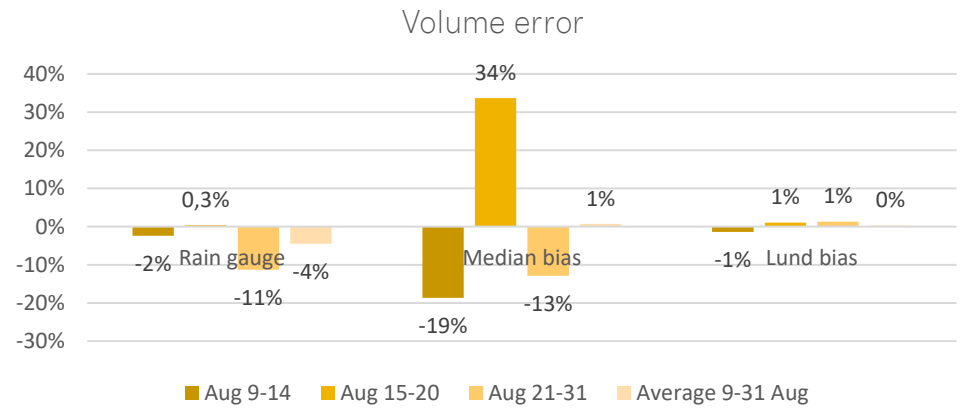

Figure 28. Volume error for the different data sets, along with the average value.

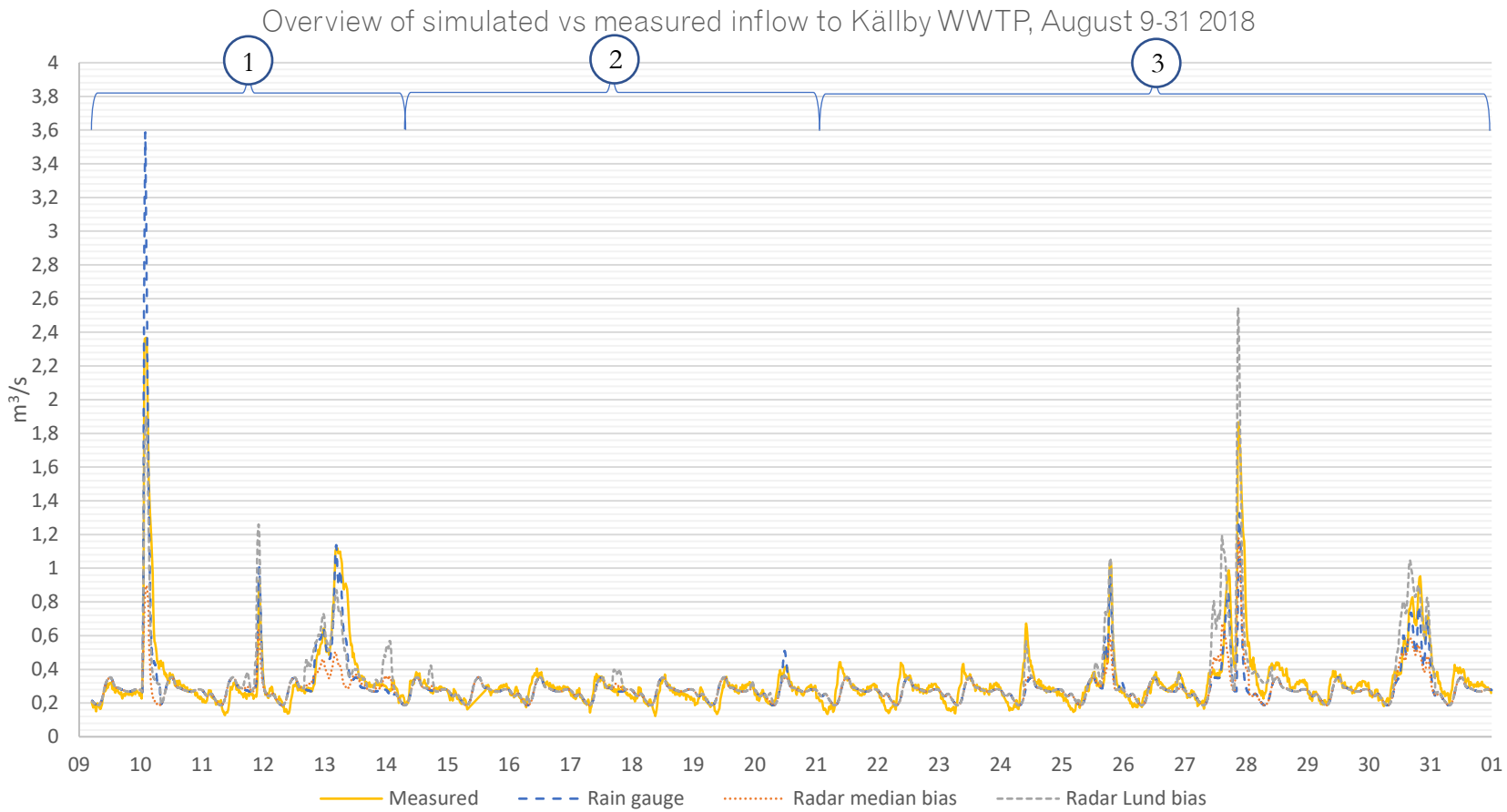

Figure 29. Overview over simulated vs measured inflow to Källby WWTP, August 9-31 2018.

5.2. Rain gauge data

5.2.1. Section 1 – August 9-14

Figure 30 shows the results of the simulation with the rain gauge data set for section 1, from August 9 to 14. As confirmed by the statistical parameters in Table 12, this section provided both a higher explained variance and a lower volume error compared to the average value of the data set. The peak error however is almost 50 % and thus higher than the average value presented in Table 11. As seen in Figure 30, the runoff peak between the 9th and the 10th was measured to more than 1 m^3/s lower than suggested by the simulation. It should be noted however, that the flow meter at the inlet of Källby WWTP has a maximum measuring capacity of 2.4 m^3/s.

Considering the flow peak between the 12th and 13th, the simulated peak value matches the measured value although the simulated flow diminishes faster than the measured flow.

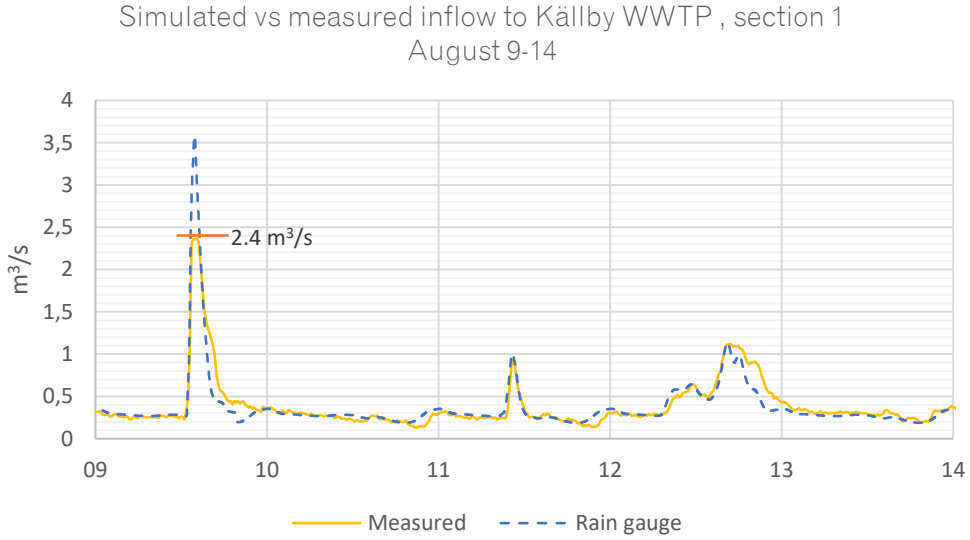

Figure 30. Simulated vs measured inflow to Källby WWTP, section 1 August 9-14.

Table 12. R2, volume error and peak error for rain gauge data in section 1.

Rain gauge data, section 1 August 9-14	
R^2	0.86
Volume error	-2 %
Peak error	48 %

5.2.2. Section 2 – August 14-20

Figure 31 shows the results of the simulation with the rain gauge data set for section 2, from August 15-20. This is a period with little rain, and it is reflected in the cyclic pattern of the both measured and simulated flows. The measured series shows more fluctuations than the simulated flow. During this period however, the precipitation data have a limited impact on the results. On the 20th of August the simulated flow results show a peak that is not reflected in the measured flow. The statistical values in Table 13 confirms that the fluctuations have a lower correlation to measured flows when limited amounts of rain are registered. The volume error is however close to zero, while the peak error is noted to 23 %, possibly related to the peak on the 20th and on the 15th, when there is a possible gap in the measured data series.

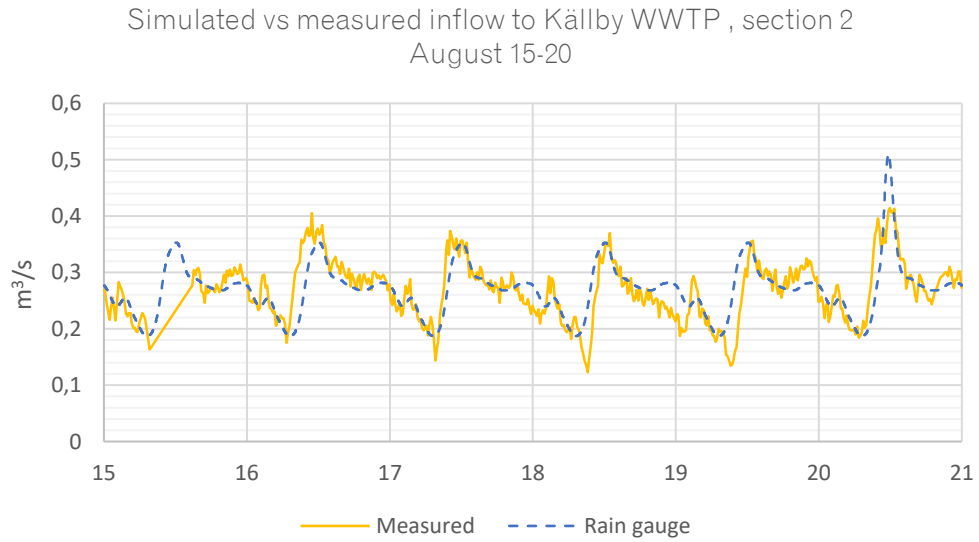

Figure 31. Simulated vs measured inflow to Källby WWTP, section 2 August 15-20.

Table 13. R2, volume error and peak error for rain gauge data in section 1.

Rain gauge data, section 2 August 15-20	
R2	0.57
Volume error	-0.3 %
Peak error	23 %

5.2.3. Section 3 – August 21-31

Figure 32 shows the results of the simulation with the rain gauge data set for section 3, from August 21-31. During this period several peaks are seen in the measured and simulated flows. On August 24, a peak is registered in the measured flow that is not captured by the simulated flow. Likewise, the second measured peak on the 27th (1.87 m^3/s) is 0.6 m^3/s higher than the simulated peak, which also diminishes faster than the measured. The triple peak on the 30th shows a similar pattern although with lower flows and smaller differences. Looking at the statistic parameters for the section (Table 14), the explained variance R^2 is again higher than in section 2, whereas the volume error and peak error show that the simulated values are underestimated compared to measured values.

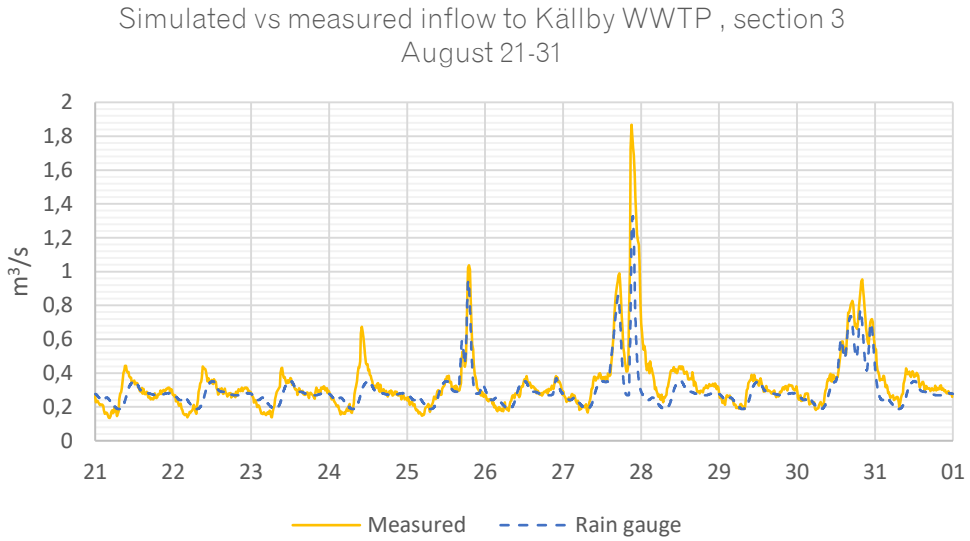

Figure 32. Simulated vs measured inflow to Källby WWTP, section 3 August 21-31.

Table 14. R2, volume error and peak error for rain gauge data in section 2.

Rain gauge data, section 3 August 21-31	
R^2	0.75
Volume error	-11 %
Peak error	-29 %

5.3. X-band radar data

This section contains a presentation of the modelling results from the X-band radar data sets. Results from both the median bias adjusted data (multiplied with a factor 0.2536) and the Lund bias adjusted data (multiplied with a factor 0.7293) are shown in comparison to the measured flows. As with the rain gauge results, the radar data results are presented section-wise.

5.3.1. Section 1 – August 9-14

Figure 33 shows the results of the simulation with the radar data set for section 1, from August 9 to 14. Overall, the flow from the data adjusted with the median bias show lower peak values than both measured flows and flows simulated with Lund bias adjusted data. The Lund bias adjusted data underestimates the peak around midnight the 10th but overestimates the peak between the 11th and 12th. Regarding the peak on the 13th, the Lund bias adjusted data shows an underestimation. The measured flow diminishes faster and show no peaks after the 13th at noon, as a contrast to the flow simulated with the Lund bias adjusted data.

The statistical parameters in Table 15 suggest that the correlation is lower for the median bias adjusted data than for the Lund bias adjusted (0.63 compared to 0.76) and that the flow volumes simulated with the median data sets are underestimated while the volumes simulated with Lund bias adjusted data were more accurate. Concerning the peaks, both data sets underestimated the flow compared to measured flow, although the flow from the median bias adjusted data set shows a larger underestimation (-62 % compared to -20 %).

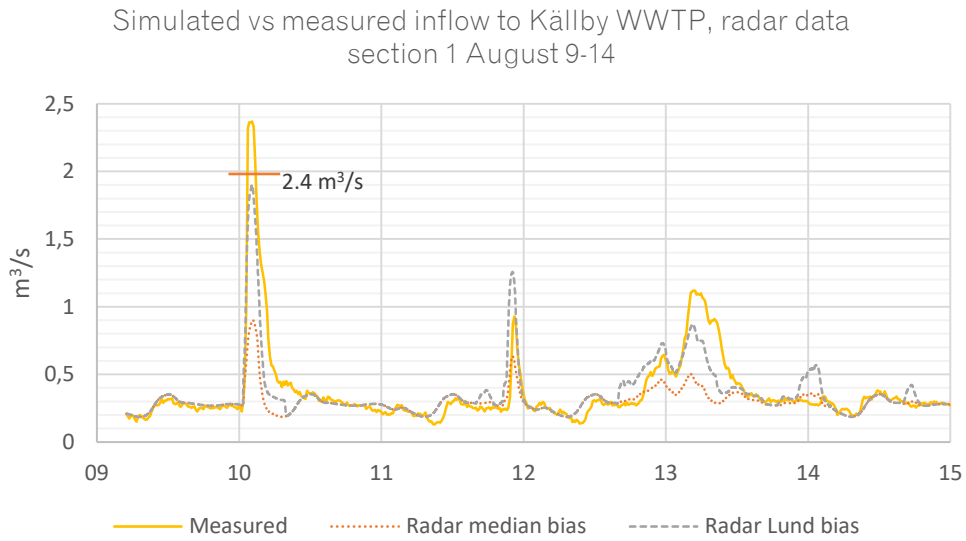

Figure 33. Simulated vs measured inflow to Källby WWTP with radar data, section 1 August 9-14.

Table 15. R2, volume error and peak error for rain radar data in section 1.

Radar data, section 1 August 9-14	Median bias adjusted	Lund bias adjusted
R^2	0.63	0.76
Volume error	-19 %	-1 %
Peak error	-62 %	-20 %

5.3.2. Section 2 – August 15-20

Figure 34 shows the results of the simulation with the radar data set for section 2, from August 15 to 20. Similarly to the rain gauge results of this section, little rain has affected these simulated results and these flows are therefore mainly based on the cyclic wastewater background flows. However, the radar data based flow show one small peak on the 17th that is not reflected in the measured data series. The shape is similar to the two radar data sets, but as in section 1 the Lund bias adjusted data produce a higher peak.

The statistical parameters are found in Table 16.

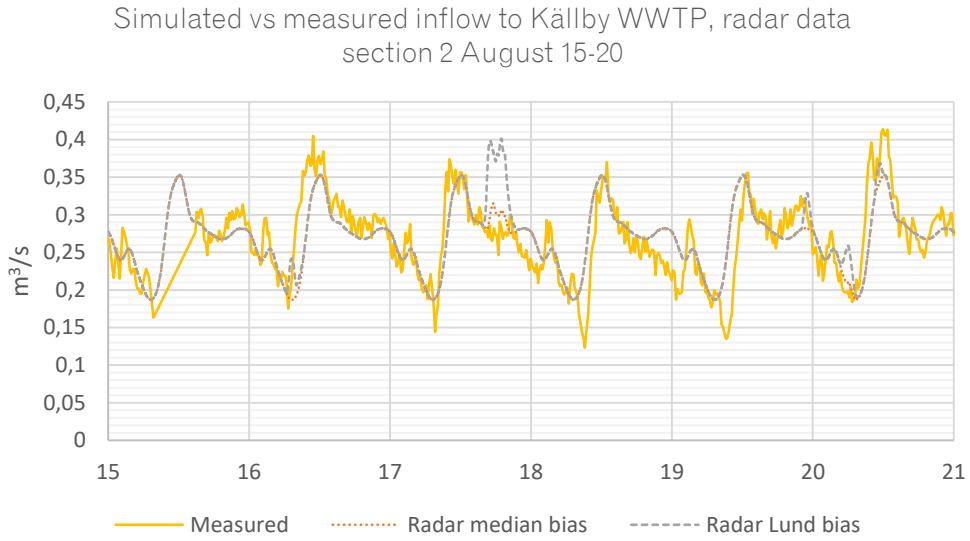

Figure 34. Simulated vs measured inflow to Källby WWTP with radar data, section 2 August 15-20.

Table 16. R2, volume error and peak error for rain radar data in section 2.

Radar data, section 2 August 15-20	**Median bias adjusted**	**Lund bias adjusted**
R^2	0.55	0.44
Volume error	34 %	1 %
Peak error	-15 %	2 %

5.3.3. Section 3 – August 21-31

Figure 35 shows the results of the simulation with the radar data set for section 3, from August 21 to 31. The overall trend is similar to the two previous sections; the flows simulated with median bias adjusted radar data are lower than the measured flows and the flows from the Lund bias adjusted radar data. The peaks on the 24th and 25th are captured with a high accuracy by the Lund bias adjusted simulated flows, whereas the peaks and from the 27th to the 31st are overestimated and diminishes slower than the measured flow values.

Looking at the statistical parameters in Table 17, the explained variance almost reaches 0.75 for both data sets and the Lund adjusted data set shows a volume error of only 1 %. The peak errors are of the same magnitude for the two data set, but with different signs; the median adjusted data show an underestimation of 38% while the Lund adjusted overestimates by 34%.

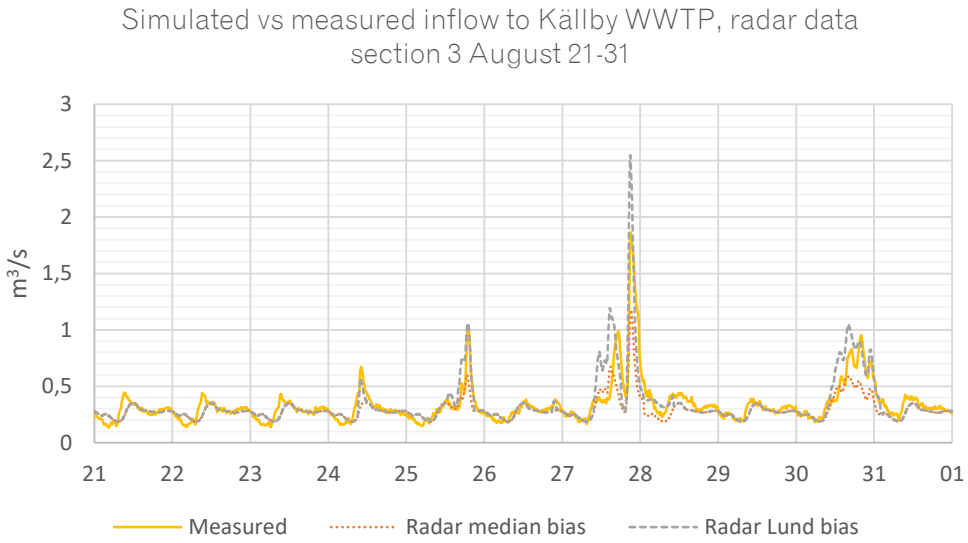

Figure 35. Simulated vs measured inflow to Källby WWTP with radar data, section 3, August 21-31.

Table 17. R2, volume error and peak error for rain radar data in section 3.

Radar data, section 2 August 15-20	**Median bias adjusted**	**Lund bias adjusted**
R^2	0.73	0.74
Volume error	-13%	1 %
Peak error	-38 %	34 %

5.4. Comparative analysis of highlighted events

Five of the above presented events are highlighted and analyzed in this section. The type and quality of the input data form the base of the analysis.

5.4.1. August 10

Figure 36 shows the measured and simulated inflow to Källby WWTP on the 10th of August 2018. This event presented the highest measured inflow value, as well as the highest simulated value with the rain gauge data. As described in section 3, the rain event on the 10th of August was of very high intensity, which caused an extensive blockage of the radar beam that resulted in little or no data for 15-30 minutes. This is one possible cause to why the Lund bias adjusted radar data flow peak reaches half the value of the rain gauge flow peak while it during other events has tended to overestimate both the measured flow peak and the rain gauge simulated flow peak.

As mentioned in section 3, the flow meter at Källby WWTP has its maximum measuring range at 2.4 m^3/s, which makes it difficult to evaluate how close to the real flow the rain gauge simulation was.

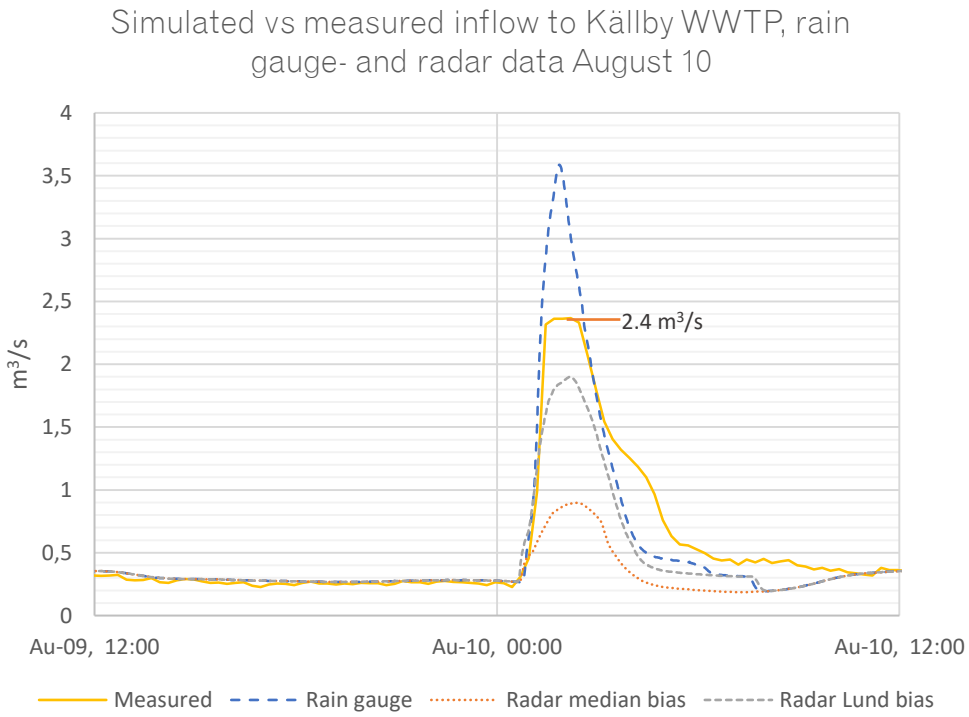

Figure 36. Simulated vs measured inflow to Källby WWTP on August 10, all three data sets.

5.4.2. August 13

Figure 37 shows the measured and simulated inflow to Källby WWTP on the 13th of August 2018. This precipitation event lasted, with mainly low intensity, for several hours and the radar registered rainfall during a longer period than the rain gauge. It can be noted that the Lund bias adjusted data show an earlier rise in flow than the measured and rain gauge simulated flows. Simulated flows from both rain gauge data and radar data diminishes faster than the measured data and the peaks of the radar data are both lower than measured and rain gauge values. Around midnight on the 14th, a small peak is registered in the flow simulated on the Lund bias adjusted data, that is not registered in either measured flow or rain gauge simulated flow.

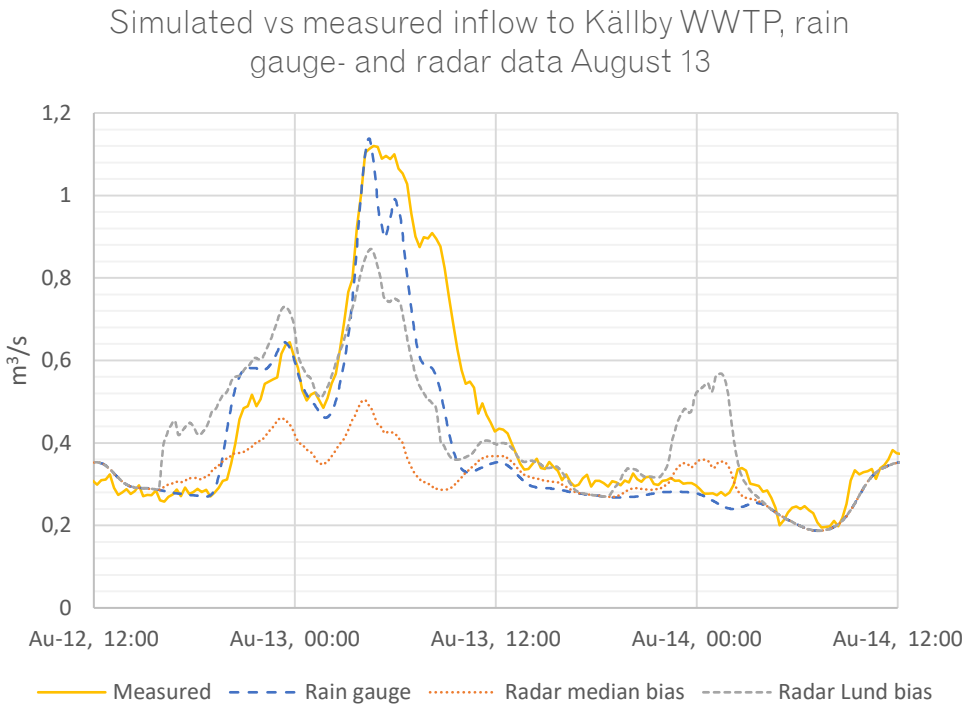

Figure 37. Simulated vs measured inflow to Källby WWTP on August 13, all three data sets.

5.4.3. August 24

On the 24th of August, a small but clear flow peak was registered by the flow meter at Källby WWTP (Figure 38). This peak was captured by the simulated flow from the Lund bias adjusted radar data, although slightly underestimated. It was not, however captured by the flow from the median adjusted radar data, nor by the flow from the rain gauge data.

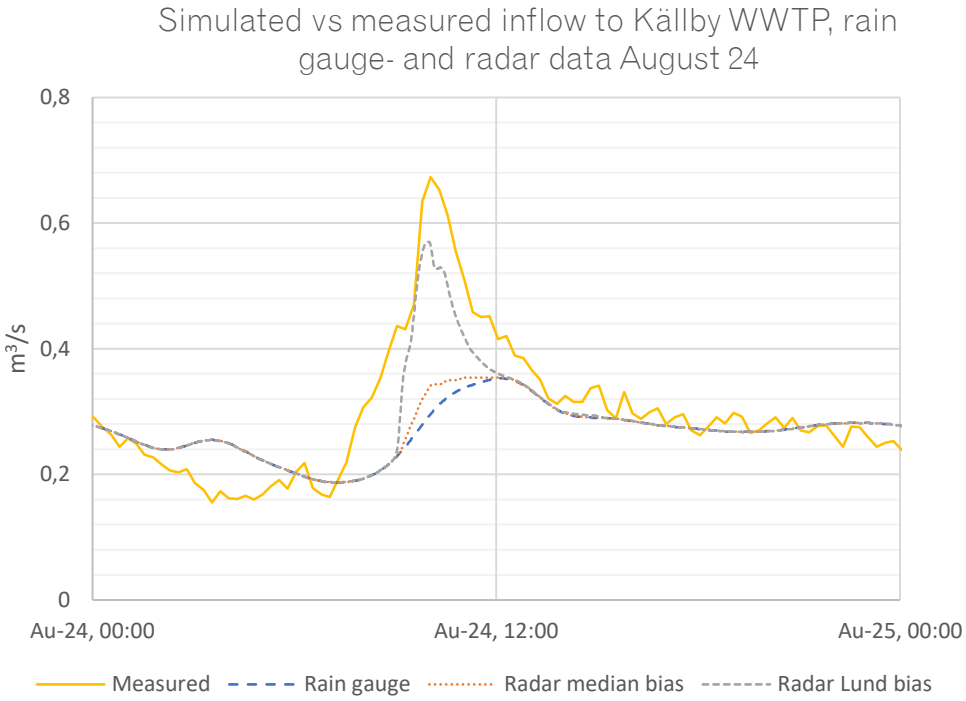

Figure 38. Simulated vs measured inflow to Källby WWTP August 2, all three data sets..

5.4.4. August 27-29

Figure 39 shows the simulated vs measured flow for all three data sets on the 27th of August. Two clear peaks are seen in the measured data set, where the earlier peak measures almost half the second peak (1 m^3/s compared to 1.8 m^3/s). This is reflected in the simulated time series as well although the Lund bias adjusted data flow simulates an earlier start (analogous to the situation on the 13th). The higher peak in this data set is also almost 1 m^3/s higher than the measured peak. In this peak, the rain gauge data and median adjusted radar data flow sets are close, while the rain gauge flows in other situations tend to be higher than the median adjusted radar data flows.

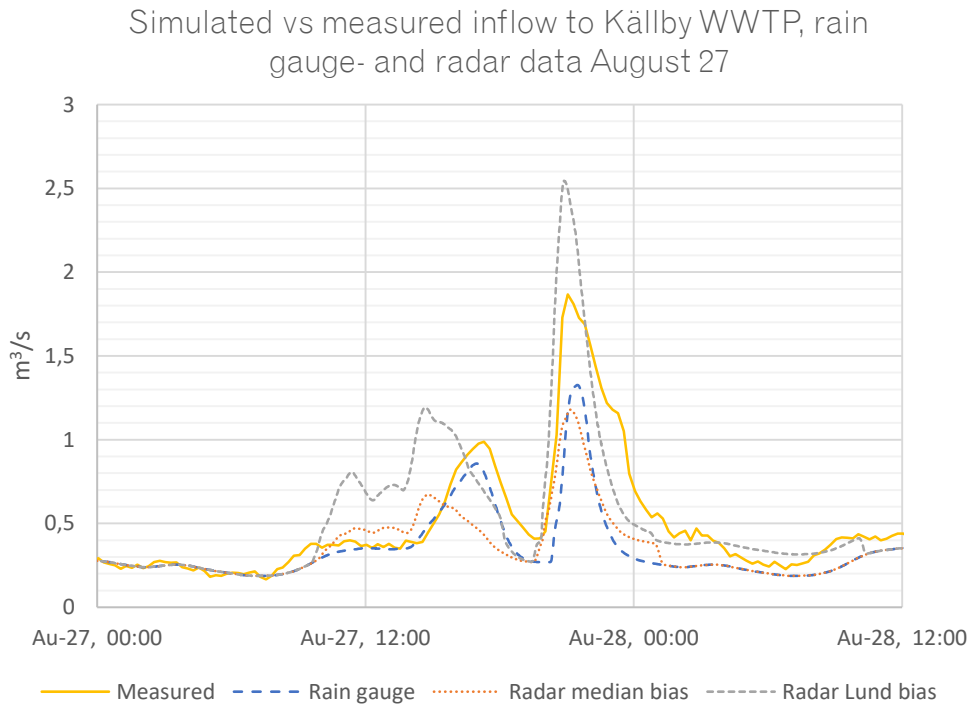

Figure 39. Simulated vs measured flow to Källby WWTP, August 27, all three data sets.

5.4.5. August 30

The flows simulated after the rain event in the morning on the 30th of August show again that the flow based on the Lund bias corrected radar data set is overestimated in the beginning compared to the measured flows, although the overall shape is similar (Figure 40).

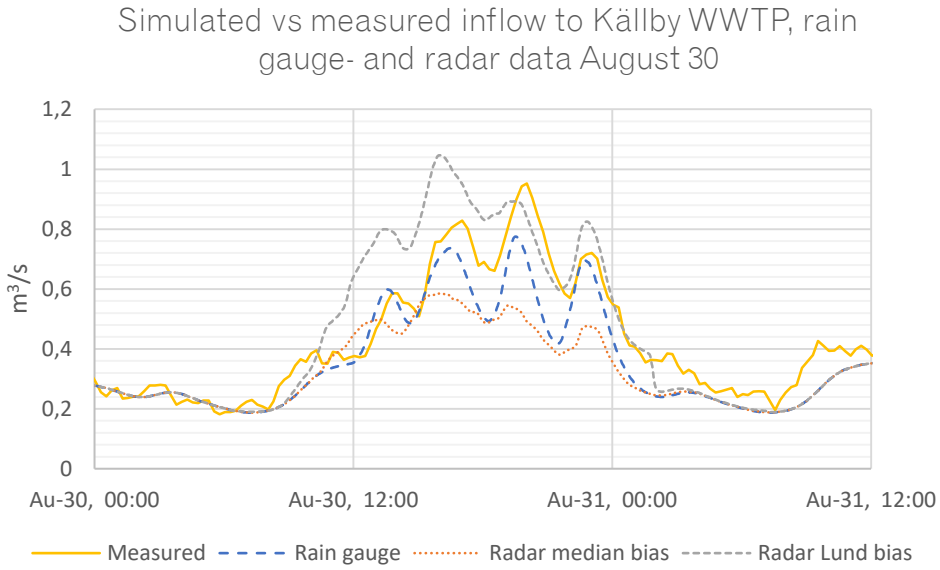

Figure 40. Simulated vs measured inflow to Källby WWTP on August 30, all three data sets.

5.4.6. Concluding analysis

Based on the results presentation in general, and in this comparative analysis in particular, a few concluding observations can be made:

a) Lund coefficient (0.7293) adjusted data set tends to produce overestimated peak flows, while the median coefficient (0.2536) adjusted data set tends to produce underestimated flows.
b) Low intensity rainfall tends to generate an early start of increased flow in the Lund adjusted data set.
c) The Lund adjusted values show low volume errors, around 0 %.
d) Beam attenuation at high intense rainfalls has an impact on the simulated flows, which are then underestimated.
e) With X-band radar data it is possible to capture flow peaks that are not registered by the rain gauge simulated flow.

These observations form the basis in the following discussion, aiming to draw further conclusions to the questions stated in section 1.

6. Discussion

In this section the points from the previously concluding analysis of the simulation results are discussed, along with the usage and possibility of the radar and its data.

6.1. X-band radar data as input data

6.1.1. Raw data and bias adjustment

The raw data downloading and processing to make it suitable for the MIKE urban model was a time-consuming work, as much needed to be performed manually. In cases when the grid cell in the webtool used for downloading the radar data did not match the grid cell overlaying the catchment in ArcMap it is possible that both the wrong grid cell was assumed to affect the catchment and that the weighting coefficient was over- or underestimated. This mismatch would in these cases mainly have affected smaller fractions of the grid cell and the effect is likely to be minor. To avoid this risk however, and to make it possible to read radar data in near real time this procedure would need to be automatically run by an algorithm in the future situation of online operation.

When downloading the radar data, it was also noted that for several cells in the central parts of Lund city there were few registered data points. One data point represented one minute of registered precipitation, and thus lower rain amounts were noted here compared to other catchments. The large spread in the radar data completeness shown in section 3 makes it likely that there was precipitation that the radar did not register. As mentioned in the same section, an important part of the central parts of Lund were suffering from radar noise disturbing the signal and where the applied noise filter eliminated all data in the pixels where noise was present. A consequence of this – apart from that rain data were missing – could be that the procedure of determining a relevant bias correction factor resulted in a misleading factor. Afterall, the bias correction factor determined with the Lund rain gauge data were almost a factor three compared to the median correction factor, possibly due to that the grid cell where the rain gauge is placed suffered from radar noise. Despite this, the Lund data series showed the lowest volume errors of the three data series. Since the Lund factor was determined based on the most local of the included rain gauges it would have been more likely to assume that this would have shown a corrected data series with high correlation to the rain gauge series. As seen in section 3 there was instead a large spread in the accumulated values amongst the Lund bias adjusted time series. If nothing else, this gives an indication of that several rain gauges would be needed in order to improve the bias correction coefficient.

In the raw precipitation data it was seen that for high intensity rainfalls, the start- and end times of the event were rather well correlated between the radar and the rain gauge, which was reflected also in the simulated flow. Although the peak value differed from the two data sets and compared to the measured flow, the shape and timing were similar. The same cannot be said considering the low intensity rainfalls, where the radar in some cases registered data hours before and/or after the rain gauge. This could be partly due to the radar measuring precipitation high above ground; at low intensity rainfall the raindrops may be more likely to drift away or evaporate before reaching the rain gauge. Another possibility could be that the drops generally are lighter than during high intensity rain, resulting in a slower descent towards ground. The rain gauge itself is not faultless, for example since the tipping-bucket type used by VA SYD needs to be filled with 0.2 mm before anything is registered. When the first tip is registered, it is not possible to see when the first raindrop really hit the gauge. At a low intensity rainfall it may take several minutes before the little bucket is filled, and in the same way the rain may continue for several minutes after the last tip was registered. If the weather is warm, the little rain that hit the rain gauge might also evaporate. Since the low intensity rainfall is connected to these measurement uncertainties, it was perhaps not surprising that the simulated flows showed less correlation.

Another factor affecting the radar data is the scan level. The data used in this project were level 2 data and it is possible that the results would have differed if for example level 3 would be used. If the level is too low, it is easily blocked and disturbed by tall buildings and an elevated landscape. A too high level does on the other hand not reach low enough to capture a fair image of the rainfall – which could increase these recently discussed issues with the low intensity rainfall. For future studies it would therefore be interesting to investigate which scan level that gives the optimal performance, or if an interpolation could be an alternative.

6.1.2. Strengths and weaknesses

A clear strength of the X-band radar was seen on the 24th of August, when a flow peak was captured by the simulated flow of the radar data but not of the rain gauge data. Looking at a snapshot from the rain event (Figure 41), it is seen that

(despite the lack of data in the central parts due to noise filter), the highest rain intensities did not pass by the rain gauge (circled) and thus there were not enough rain registered to simulate the flow peak. This rain event was relatively short and without exceptionally high intensities, but it shows the potential strength of measuring rainfall with a high spatial and temporal resolution within an urban area.

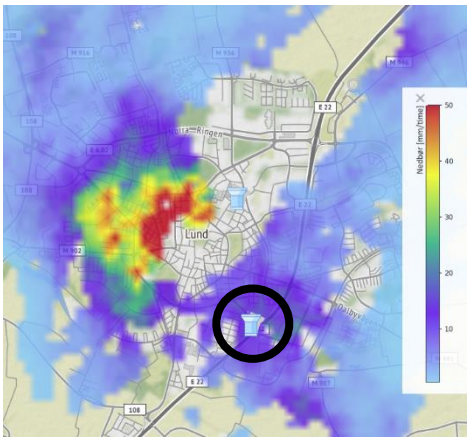

Figure 41. Snapshot of a rain event on the 24th of August.

Considering high intensities, one of the most significant weaknesses with the X-band radar was noted on the 10th of August. Figure 42 shows a snapshot from the event, with the Dalby X-band radar image at the front and the SMHI C-band radar image at the back. The Lund rain gauge is again circled. While the rain gauge continued to capture high rain amounts, the radar beam was weakened and blocked and did not reach farther than a few kilometers. This was probably the cause to the underestimated radar flow peak in Figure 36. As previously mentioned in the Background section, this problem could be at least partially solved if the X-band radar is connected to a network of other radars. In the case of an online control, it is not desired to risk feeding the models with beam blocked data during high intensity rainfalls.

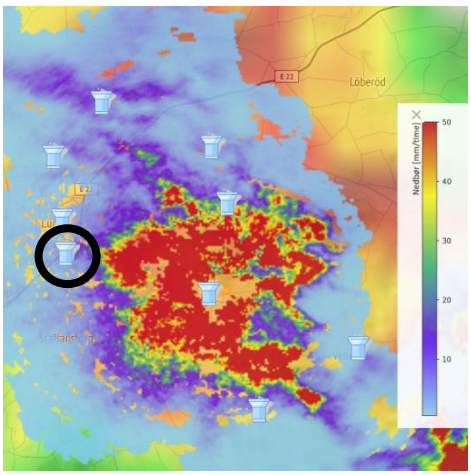

Figure 42. Snapshot from the high intensity rain event on the 10th of August.

Another weakness is the sensitivity to noise, seen in Figure 41. For the radar to produce reliable data to an online control model, it is necessary to assure that the radar data is filtered in such a manner that only noise and not real precipitation data points are removed. This is however likely to need more available data than what was produced during this test period.

As the radar continuously monitors its surroundings and produces new data every minute, it gives valuable information on how the rainfall is moving in a more detailed manner than what the rain gauge network captures. The higher spatial

resolution of the X-band radar compared to the SMHI C-band radar is said to more accurately capture local, high intensity rainfalls with an uneven distribution within a city. It would therefore have been interesting to conduct this study with C-band radar data in order to compare if and how the simulated inflows would have varied between the two types of radar data.

6.2. Modelling

In this section the modelling procedure is discussed, focusing on the calibration period and the input data format.

6.2.1. Calibration

The MIKE urban model used in this project was designed and calibrated with rain gauge precipitation data where the spatial variability naturally is less than what is achieved with the radar data. The temporary rain gauges that where installed in Lund in Autumn 2018 therefore likely helped capturing the temporal and spatial variability of the occurring rainfalls. This could explain why the Lund radar data flow series showed higher correlation than the rain gauge series. The study period of this project from where the rainfall data were gathered (August 2018) lies within the calibration period (July-October/February 2018/2019), which may have some impact on the results. Since the radar data make up a data set that differs from the rain gauge in its spatial and temporal spreading it could be considered as "new" data, although of course most of the rain events were registered also by the rain gauge. Unfortunately, it was not possible to run the model with radar data from Spring 2019, due to timing reasons. For another time, it would be interesting to see how the model performs with radar data from outside of the calibration period.

6.2.2. Input data format

As described in section 3, the radar data required a handful of processing steps before being ready for the model. Time series are easy to handle, but some of the advantage of the high spatial resolution of the radar is lost during the weighting procedure – especially if the catchment is widespread. If the possibility to download time series from the radar web tool persists, it would be of high interest to be able to choose to download already processed data for a specific catchment and not only for a specific grid cell. If the input data to the model would remain in a raster format, the spatial variability would also be maintained as the raster is georeferenced and a weighting simplification would not be needed. A clear drawback with the raster format of the original data is the large files – 60 MB per minute is generated. To get the most out of the online model together with the radar data, it would be needed to maintain high spatial variability and assure fast computation times.

6.3. Further questions

This final discussion section highlights further questions that need to be assessed to ensure and improve the use of the X-band radar data.

6.3.1. Seasonal variations

The testing period of the X-band radar started in the middle one of the warmest and driest summers since Swedish temperature and rainfall measurements began. These conditions are thus not truly representative for a normal summer and certainly not representative for the seasonal variations that occur during a year. Even though snowy winters are unusual this part of the country, it is not unusual with a few snow events per winter. How does the radar register snow? What happens when the precipitation is frozen on the radar scan level but liquid when it reaches the ground? Would the radar beam be weakened from a heavy snowfall in a similar way as the 10th of August? What if wet snow lands and freezes on the (unheated) radar dome? These questions could possibly be answered a year from now, when the radar has been running and collecting data during a complete year.

6.3.2. Local bias adjustment

The bias correction applied to the radar data in this project was a simple mean-field bias, based on either all of VA SYD's operating rain gauges (the median bias value) or the Lund rain gauge. With several online rain gauges within Lund city, it would be possible to capture differences on a smaller spatial scale. Perhaps it would even be possible to develop local bias correction coefficients, if the radar data would show to vary in accuracy within Lund. As the radar data proved to register light precipitation earlier than the rain gauge, a bias correction or calibration in time could be necessary.

7. Conclusions

The main purpose of this thesis study was to evaluate the usage of X-band weather radar data as input to a MIKE urban model. Although the study period was limited in time to only one month of collected data, it can be concluded that these data have their strengths and weaknesses. One of the most prominent strengths is its spatial coverage, which enabled the capture of the flow peak on the 24th of August, which was not registered when rain gauge data were used. In case of a higher intensity local rainfall this information can be of great value. One of the most prominent weaknesses, however, is the risk of beam attenuation when high intensity rainfalls pass the radar. In case an X-band radar network is implemented in the region it is of high interest to study how and if this affects the beam attenuation.

Since the study period was limited to one month, it is also possible to conclude that longer data series are needed for optimization of both noise elimination and bias adjustment. Although several catchments were represented by fewer data points due to the noise, it was clear that the radar data needed bias correction and that the median bias correction coefficient (0.2536) was too low. In most cases the Lund bias correction factor (0.7293) was however not low enough in many cases. As long as large parts of central Lund are subject to more or less significant radar noise, the data do not mirror reality and it will be difficult to apply a proper bias correction. The bias correction itself requires rain gauge data series with higher geographical spreading than what has been the case in this project. As low intensity rainfalls tend to produce flow results with less accurate timing than the high intensity rainfalls, bias correction dependent on intensity could be an alternative worth trying.

Regarding the modelling, a calibration with radar data is recommended to eliminate uncertainties that originate in the calibration data type. For the radar data to be a complementary alternative to rain gauge data in the practical use of hydrological modelling they need to be easily accessible in a format that allows the user to download georeferenced datafiles that are ready to use. In the future case of an operating online model, the data need to maintain its high spatial resolution and still be stored in files small enough to allow for fast computing times. It is also essential that the radar data used for input to either a nowcast model or directly into an online flow simulation are more accurate in time and volume than what the current radar data offer.

To summarize this, the radar data as input to a MIKE urban hydrological model do have a large potential in capturing the spatial variability of a rainfall and thus avoiding the risk of "invisible" rains that do not pass by the rain gauge. For the

radar to reach its full potential in this field, longer data series are needed in combination with a denser rain gauge network in order to solve the problem with noise and to find a suitable bias correction. With the data sets available for this project it is therefore not possible to conclude that one data set outperforms the other in terms of simulated flows. It would however be interesting, to see the results from a similar study a year or two from now.

8. References

Antonini, A. *et al.* (2017) 'On the Implementation of a regional X-bandweather radar network', *Atmosphere*, 8(2), pp. 1–20. doi: 10.3390/atmos8020025.

Blomquist, D. *et al.* (2016) *Riktlinjer för modellering av spillvattenförande system och dagvattensystem*. Available at: www.svensktvatten.se (Accessed: 20 March 2019).

Borup, M. *et al.* (2016) 'Dynamic gauge adjustment of high-resolution X-band radar data for convective rain storms: Model-based evaluation against measured combined sewer overflow', *Journal of Hydrology*, (539), pp. 687–699. doi: 10.1016/j.jhydrol.2016.05.002.

CASA (no date) *DFW Urban Test Bed - Research : UrbanTestBed*. Available at: http://www.casa.umass.edu/main/research/urbantestbed/ (Accessed: 19 February 2019).

DHI a (2017) 'Mike urban model manager'.

DHI b (2017) 'MIKE Urban CS - User guide'. Available at: http://manuals.mikepoweredbydhi.help/2017/Cities/CollectionSystem.pdf.

DHI c (2017) *MOUSE Runoff Reference Manual*. Available at: http://manuals.mikepoweredbydhi.help/2017/Cities/MOUSERunoffReference.pdf (Accessed: 1 June 2019).

EnviDan (no date) *Udviklingsprojekt Vejrradar*. Available at: https://www.envidan.dk/cases/vejrradar (Accessed: 19 February 2019).

Goormans, T. and Willems, P. (2013) 'Using Local Weather Radar Data for Sewer System Modeling: Case Study in Flanders, Belgium', *Journal of Hydrologic Engineering*, 18(2), pp. 269–278. doi: 10.1061/(ASCE)HE.1943-5584.0000589.

Haghighatafshar, S. *et al.* (2018) 'Efficiency of blue-green stormwater retrofits for flood mitigation - Conclusions drawn from a case study in Malmö, Sweden', *Journal of Environmental Management*, 207, pp. 60–69. doi: 10.1016/j.jenvman.2017.11.018.

Hedell, C. and Kalm, A. (2019) *Applying X-band radar data in urban hydrology - Adjusting data for a neural network model, based on the pilot project in Dalby 2018*. Lund University.

Hernebring, C. and Mårtensson, E. (2013) *Pluviala översvämningar: konsekvenser vid skyfall över tätorter, en kunskapsöversikt*. Available at: https://www.msb.se/RibData/Filer/pdf/26609.pdf (Accessed: 28 January 2019).

Jørgensen, A. T. *et al.* (2012) *METSAM, MiljøEffektiv Teknologi til intelligent*

SAMstyring af spildevandssystemer.

Krüger A/S (no date) *STAR Utility Solutions referencer*. Available at: http://www.kruger.dk/forsyning/avanceretonlinestyring/referencekort/ (Accessed: 26 April 2019).

Larsson, R. (2018) 'Lecture on Conceptual modelling in the LTH-course VVRN10'. Lund.

Löwe, R. *et al.* (2014) 'Probabilistic online runoff forecasting for urban catchments using inputs from rain gauges as well as statically and dynamically adjusted weather radar', *Journal of Hydrology*, 512, pp. 397–407. doi: 10.1016/j.jhydrol.2014.03.027.

Lund, N. S. V. *et al.* (2018) 'Model predictive control of urban drainage systems: A review and perspective towards smart real-time water management', *Critical Reviews in Environmental Science and Technology*. doi: 10.1080/10643389.2018.1455484.

Lundblad, U. and Backö, J. (2012) *Undersökningsmetoder för att hitta källorna till tillskottsvatten*. Available at: www.svensktvatten.se (Accessed: 19 February 2019).

Lunds kommun (2016) *Utbyggnads- och boendestrategi*.

Lunds kommun and VA SYD (2018) *Översvämningsplan för Lunds kommun*. Available at: https://www.lund.se/globalassets/regelsamling/renhallning_och_vatten/oversvamningsplan-lunds-kommun-180625-antagen-180322-kf.pdf (Accessed: 29 January 2019).

Malm, A. and Svensson, G. (2011) *Material och ålders-fördelning för Sveriges VA-nät och framtida förnyelsebehov*. Available at: www.svensktvatten.se (Accessed: 31 January 2019).

Mississippi WMO (2017) *How a Tipping-Bucket Rain Gauge Works*. YouTube. Available at: https://www.youtube.com/watch?v=ygLJV8upFQ4 (Accessed: 7 March 2019).

Naturvårdsverket (1993) *Bräddning från avloppsledningar*.

Naturvårdsverket (2018) *Rening av avloppsvatten i Sverige 2016*, *Swedish Environmental Protection Agency*. Available at: https://www.naturvardsverket.se/Documents/publikationer/978-91-620-8372-4.pdf%0Ahttps://www.naturvardsverket.se/Documents/publikationer6400/978-91-620-8629-9.pdf?pid=5493.

Nielsen, J. E., Thorndahl, S. and Rasmussen, M. R. (2013) 'Development of method for X-band weather radar calibration', *Journal of Hydroinformatics*, 15(4),

pp. 1326–1339. doi: 10.2166/hydro.2013.126.

Nielsen, J. E., Thorndahl, S. and Rasmussen, M. R. (2014) 'Improving weather radar precipitation estimates by combining two types of radars', *Atmospheric Research*. doi: 10.1016/j.atmosres.2013.12.013.

O'Donnell, E. C., Lamond, J. E. and Thorne, C. R. (2017) 'Recognising barriers to implementation of Blue-Green Infrastructure: a Newcastle case study', *Urban Water Journal*. Taylor & Francis, 14(9), pp. 964–971. doi: 10.1080/1573062X.2017.1279190.

Pedersen, L. (2009) *Identification and Quantification of Uncertainties Related to Using Distributed X-band Radar Estimated Precipitation as input in Urban Drainage Models*. Technical University of Denmark.

Persson, M. (2018) 'Excercise on rainfall runoff modelling'.

Pollock, M. D. *et al.* (2018) 'Quantifying and Mitigating Wind-Induced Undercatch in Rainfall Measurements', *Water Resources Research*, 54(6), pp. 3863–3875. doi: 10.1029/2017WR022421.

RainGain (2012) *FAQs Site RainGain*. Available at: http://www.raingain.eu/en/faqs (Accessed: 19 February 2019).

Salomonsson, M. *et al.* (2017) *Beredskapsplanering för skyfall.*

SCB (2018) *Kommunfakta - tätort Lund*. Available at: https://www.lund.se/globalassets/lund.se/kom_pol/kommunfakta/scb_kommunfakta/1281-lund-tatort.pdf (Accessed: 28 February 2019).

Semadeni-Davies, A. *et al.* (2008) 'The impacts of climate change and urbanisation on drainage in Helsingborg, Sweden: Combined sewer system', *Journal of Hydrology*, 350, pp. 100–113. doi: 10.1016/j.jhydrol.2007.05.028.

Shroder, J. (2016) *Transboundary Water Resources in Afghanistan*. Elsevier Inc. doi: 10.1016/B978-0-12-801886-6.00011-2.

SMHI a (2013) *Om forskning atmosfärisk fjärranalys*. Available at: https://www.smhi.se/forskning/forskningsomraden/atmosfarisk-fjarranalys/om-forskning-atmosfarisk-fjarranalys-1.254 (Accessed: 13 March 2019).

SMHI a (2017) *Antalet fall med kraftig dygnsnederbörd.* Available at: https://www.smhi.se/klimat/klimatet-da-och-nu/klimatindex/antalet-fall-med-kraftig-dygnsnederbord-1.76946 (Accessed: 31 January 2019).

SMHI a (2018) *Hur mäts nederbörd?* Available at: https://www.smhi.se/kunskapsbanken/meteorologi/hur-mats-nederbord-1.637

(Accessed: 7 March 2019).

SMHI b (2017) *Största dygnsnederbörd*. Available at: https://www.smhi.se/klimat/klimatet-da-och-nu/klimatindex/storsta-dygnsnederbord-1.76922 (Accessed: 31 January 2019).

SMHI c (2017) *Så gör SMHI en väderprognos*. Available at: https://www.smhi.se/kunskapsbanken/meteorologi/sa-gor-smhi-en-vaderprognos-1.4662 (Accessed: 26 April 2019).

SMHI e (2018) *Korta nederbördsprognoser-KNEP | SMHI*. Available at: https://www.smhi.se/forskning/forskningsomraden/meteorologi/korta-nederbordsprognoser-knep-1.414 (Accessed: 25 April 2019).

Sörensen, J. (2018) *Urban, pluvial flooding*. Lund University. Available at: http://portal.research.lu.se/portal/files/49609065/Sorensen_Thesis_Urban_pluvial_flooding.pdf (Accessed: 30 January 2019).

South, N. *et al.* (2019) *Väderradarteknik inom VA- området – test av metodik*.

Svenskt Vatten (2016) *Avledning av dag-, drän-och spillvatten*. Available at: http://vav.griffel.net/filer/P110_del1_web_low_180320.pdf (Accessed: 25 January 2019).

Sweden Water Research (no date) *Future City Flow*. Available at: https://www.swedenwaterresearch.se/en/projekt/future-city-flow-3/ (Accessed: 19 February 2019).

Thörn, P., Ekholm, H. M. and Nilsson, Å. (2017) *Klimatanpassning 2017 - så långt har kommunerna kommit*. Available at: www.ivl.se (Accessed: 31 January 2019).

Thorndahl, S. *et al.* (2013) 'Comparison of short-term rainfall forecasts for model-based flow prediction in urban drainage systems', *Water Science & Technology*, pp. 472–478. doi: 10.2166/wst.2013.274.

Thorndahl, S. *et al.* (2017) 'Weather radar rainfall data in urban hydrology', *Hydrology and Earth System Sciences*. [European Geophysical Society], pp. 1359–1380.

VA SYD (2018) *Åtgärdsplan för Lunds avlopp 2017*. Available at: www.vasyd.se (Accessed: 28 January 2019).

VA SYD (2019) *Om VA SYD*. Available at: https://www.vasyd.se/Artiklar/Om-VA-SYD/Om-VA-SYD (Accessed: 1 March 2019).

VA SYD, discussion (2019) 'Discussion'.

Vanrolleghem, P. A., Benedetti, L. and Meirlaen, J. (2005) 'Modelling and real-

time control of the integrated urban wastewater system', *Environmental Modelling & Software*, 20, pp. 427–442. doi: 10.1016/j.envsoft.2004.02.004.

Vezzaro, L. and Grum, M. (2014) 'A generalised Dynamic Overflow Risk Assessment (DORA) for Real Time Control of urban drainage systems', *Journal of Hydrology*, pp. 292–303. doi: 10.1016/j.jhydrol.2014.05.019.

VISS (2018) *Vattenkartan*. Available at: https://ext-geoportal.lansstyrelsen.se/standard/?appid=1589fd5a099a4e309035beb900d12399 (Accessed: 17 April 2019).

Wang, Y. and Chandrasekar, V. (2010) 'Quantitative precipitation estimation in the CASA X-band Dual-Polarization radar network', *Journal of Atmospheric and Oceanic Technology*, 27(10), pp. 1665–1676. doi: 10.1175/2010JTECHA1419.1.

Wennberg, C., Nordlander, H. and Hernebring, C. (2017) *Omfattning av bräddning i svenska kommuner*. Available at: www.svensktvatten.se (Accessed: 31 January 2019).

WMO (2014) *Guide to Meteorological Instruments and Methods of Observation*. Available at: https://library.wmo.int/doc_num.php?explnum_id=4147 (Accessed: 11 March 2019).

9. Appendix

The appendix contains one table with characteristics of the different catchments, where zero imperviousness implies that the catchment is connected to a separated sewage system and the storm water does not enter the wastewater pipes. A map of the catchment locations in Lund city is also provided.

Appendix table 1. Area and imperviousness of the different catchments.

Nbr	Catchment	Area [ha]	% of total catchment area	Imperviousness (%)
1	Brunnshög	99	2.8	0
2	Centrum N - Ideon	143	4.0	1
3	Centrum S	60	1.7	14.15
4	Centrum V	68	1.9	4.63
5	Centrum Ö	62	1.8	30.81
6	Dalby	382	10.8	0
7	Gastelyckan	164	4.6	0
8	Gunnesbo - Nöbbelöv N	139	3.9	0.46
9	Gunnesbo - Nöbbelöv S	235	6.6	2.72
10	Klostergården	173	4.9	0
11	Kobjer	76	2.2	6.05
12	Källby	34	1.0	12.78
13	Lerbäck	44	1.3	4.5
14	Lilla Råby	22	0.6	1.92
15	Linero	385	10.8	0.01
16	Lyckebacken	10	0.3	0
17	Möllevången	97	2.7	3.08
18	Nilstorp	80	2.3	7.73
19	Norra Fäladen N	94	2.6	5
20	Norra Fäladen S	148	4.2	1.35
21	Papegojlyckan V	100	2.8	12.41
22	Pålsjö-Tuna	201	5.7	6.46
23	Stampelyckan	38	1.1	7.37
24	Vallkärra-Stångby	219	6.2	0
25	Vipeholm	62	1.7	2.03
26	Värpinge - Nova	162	4.6	0
27	Väster	55	1.5	23.16
28	Östra Torn N	124	3.5	0.3
29	Östra Torn S	73	2.1	1.37

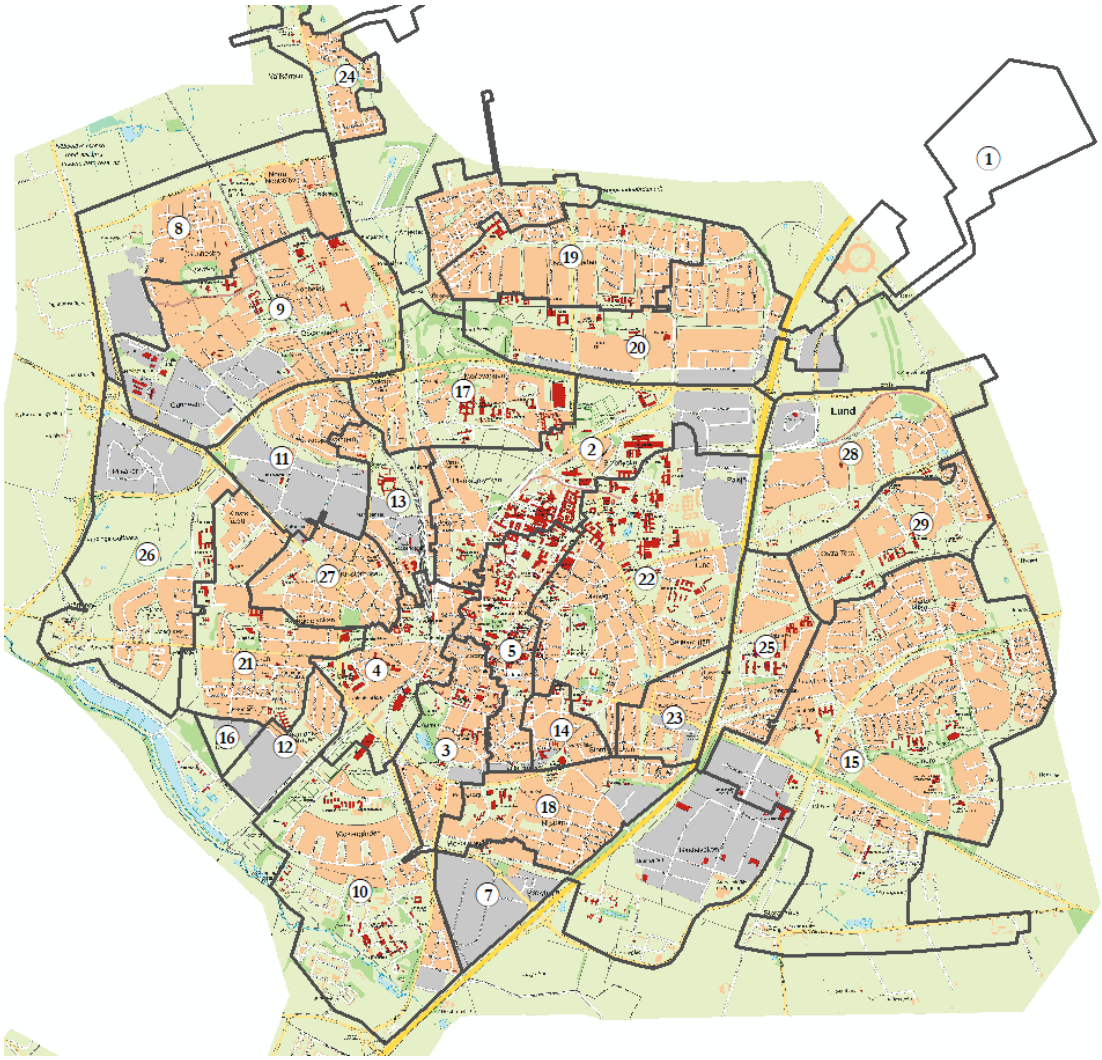

Appendix figure 1. Location of the different catchments in the model. Catchment 6 covers Dalby, east of Lund